A SOFIA/FORCAST Grism Study of the Mineralogy of Dust in the Winds of Proto-planetary Nebulae

RV Tauri Stars and SRd Variables

http://arxiv.org/abs/1706.00445

Ryan Arneson (University of Minnesota)

R. Gehrz, C. Woodward, A. Helton, D. Shenoy, A. Evans, L. Keller, K. Hinkle, M. Jura, T. Lebzelter, C. Lisse, M. Rushton, J. Mizzrachi

Introduction

- RV Tauri stars, Population II Cepheids with spectral types F—K
- Semi-regular, bimodal variability with 30 - 150 day pulsations
- Two photometric classes
    - a: Constant mean magnitude
    - b: Varying mean magnitude (600 - 1500 days)
- Three spectroscopic classes
    - A: Types G—K, strong absorption lines and normal CH and CN bands
    - B: Type F, weaker lines and enhanced CH and CN bands
    - C: Type F, weak lines and normal CH and CN bands (Pop II)
- Atmospheres show 'depletion' phenomenon (i.e. low refractory abundances)
- SRd variables are similar but lack regular pulsations—single star systems

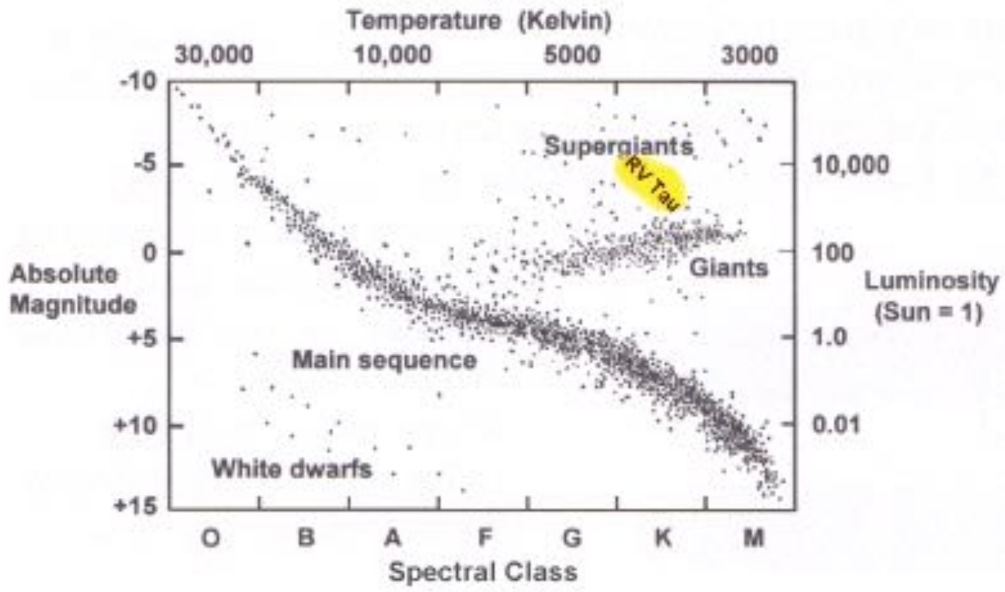

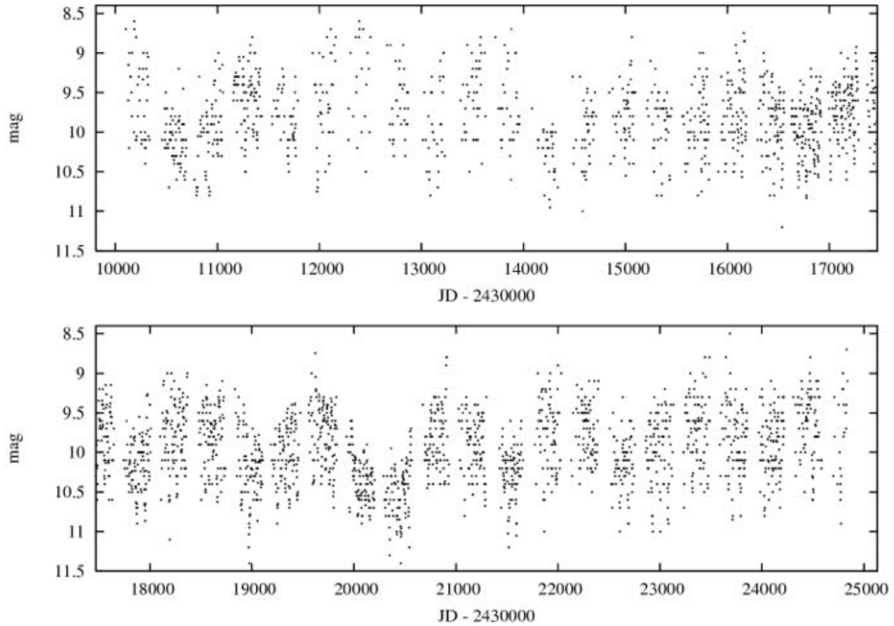

RV Tau Light Curve; Credit: AAVSO

Aims and Methods

- Determine the mineralogy content of a sample of post-AGB stars believed to be precursors to pre-planetary nebulae

- Estimate the grain size and dust temperature

- Obtained SOFIA FORCAST grism spectra between 5-40 μm for 15 RV Tauri and 3 SRd variable stars

- Achieve this using a Non-negative Least Squares spectral decomposition model

Observations

- Obtained during Cycles 2, 3, and 4; March 2014 - July 2016
- Faint Object infraRed CAmera for the SOFIA Telescope (FORCAST)
- First Light Infrared TEst CAMera (FLITCAM) observations of U Mon and RV Tau R=860 between 2.779-4.074 μm
- Grisms: G1 (4.9-8.0 μm); G3 (8.4-13.7 μm);
  G5 (17.6-27.7 μm); G6 (28.7-37.1 μm)
  R ~ 200

Name	Type	Spectral Type	Period (d)[a]	$[Fe/H]_0$[b]	PC[c]	SC[c]	SED[d]	T_{eff}(K)	Binarity[e]	Chemical Type[f]	Ref.
TW Cam	RV	F8IbG8Ib	87	-0.40	a	A	Disk	4800			1
UY CMa	RV	G0	114	-0.50	a	B		5500			2
o^1 Cen	SRd	G3Ia0	200								3
RU Cen	RV	A7IbG2pe	65	-1.10	a	B	Disk	6000	Y		4, 5
SX Cen	RV	F5G3/5Vp	33	-0.30	b	B	Disk	6250	Y		4, 5
SU Gem	RV	F5M3	50	0.00	b	A	Disk	5250			6
AC Her	RV	F2pIbK4e	75	-0.90	a	B	Disk	5900	Y	O	7
V441 Her	SRd	F2Ibe	70				Disk		Y	O	8, 9
U Mon	RV	F8IbeK0pIb	91	-0.50	b	A	Disk	5000	Y	O	1, 10
CT Ori	RV	F9	136	-0.60	a	B	Disk	5500			10, 11
TV Per	SRd	K0	358								12
TX Per	RV	Gp(M2)K0e(M2)	78	-0.60	a	A		4250			6
AR Pup	RV	F0IF8I	76	0.40	b	B	Disk	6000		O	10, 13
R Sge	RV	G0IbG8Ib	71	0.10	b	A	Disk	5100			13
AI Sco	RV	G0K2	71	-0.30	b	A	Disk	5300		C?	2, 10
R Sct	RV	G0IaeK2p(M3)Ibe	147	-0.20	a	A	Uncertain	4500			1
RV Tau	RV	G2IaeM2Ia	79	-0.40	b	A	Disk	4500		C	1
V Vul	RV	G4eK3(M2)	76	0.10	a	A	Disk	4500			2, 6

[a] Pulsation period in days

[b] The estimated initial metallicity obtained via the Zn or S abundance (Gezer et al. 2015)

[c] Photometric class (PC) and spectroscopic class (SC)

[d] Spectral energy distribution classification from Gezer et al. (2015)

[e] Y indicates confirmed binarity based on radial velocity measurements. Confirming binarity using this method is difficult because the photospheres of these variables have large amplitude radial pulsations.

[f] Stellar chemical type from He et al. (2014) and references therein

References—(1) Giridhar et al. (2000); (2) Giridhar et al. (2005); (3) O'Connell (1961); (4) Maas et al. (2002); (5) Maas et al. (2005); (6) Rao & Giridhar (2014): (7) Giridhar et al. (1998); (8) Waters et al. (1993); (9) de Ruyter et al. (2006); (10) Kiss et al. (2007); (11) Gonzalez et al. (1997b); (12) Payne-Gaposchkin (1952); (13) Gonzalez et al. (1997a)

Model

$$\lambda F_\lambda \sim \sum_i c_i \mu_i \times \sum_j a_j \lambda B_\lambda(T_j)$$

c, volume fraction of dust component

μ (μm^{-1}), absorption coefficient

a_j , scalling factor for j^{th} Planck function

B_λ ($W\ sr^{-1}\ m^{-3}$), Planck function at temperature T_j

$$\chi^2_{\rm red} = \frac{1}{N-M} \sum_{i=1}^{N} \left| \frac{F_{\rm model}(\lambda_i) - F_{\rm obs}(\lambda_i)}{\sigma_i} \right|^2$$

N, number of wavelength points

M, number of fit parameters

F_{model}, model flux at a given wavelength

F_{obs}, observed flux at a given wavelength

σ, absolute error at a given wavelength

Procedure and Monte Carlo

$$\lambda F_\lambda \sim \sum_i c_i \mu_i \times \sum_j a_j \lambda B_\lambda(T_j)$$

- Fit Planck functions to continuum
- Find dust volume fractions using a Non-Negative Least Squares Fit
- Estimate errors on the dust volume fractions from 5000 realizations of a Monte Carlo simulation

Cosmic Silicates

- Olivine ($Mg_{2(1-x)}Fe_{2x}SiO_4$) and Pyroxene ($Mg_{1-x}Fe_xSiO_3$) are the most common species
- O-Si-O bending and Si-O stretching produce IR features
- Amorphous vs. Crystalline
- Crystalline material is ~10-15%

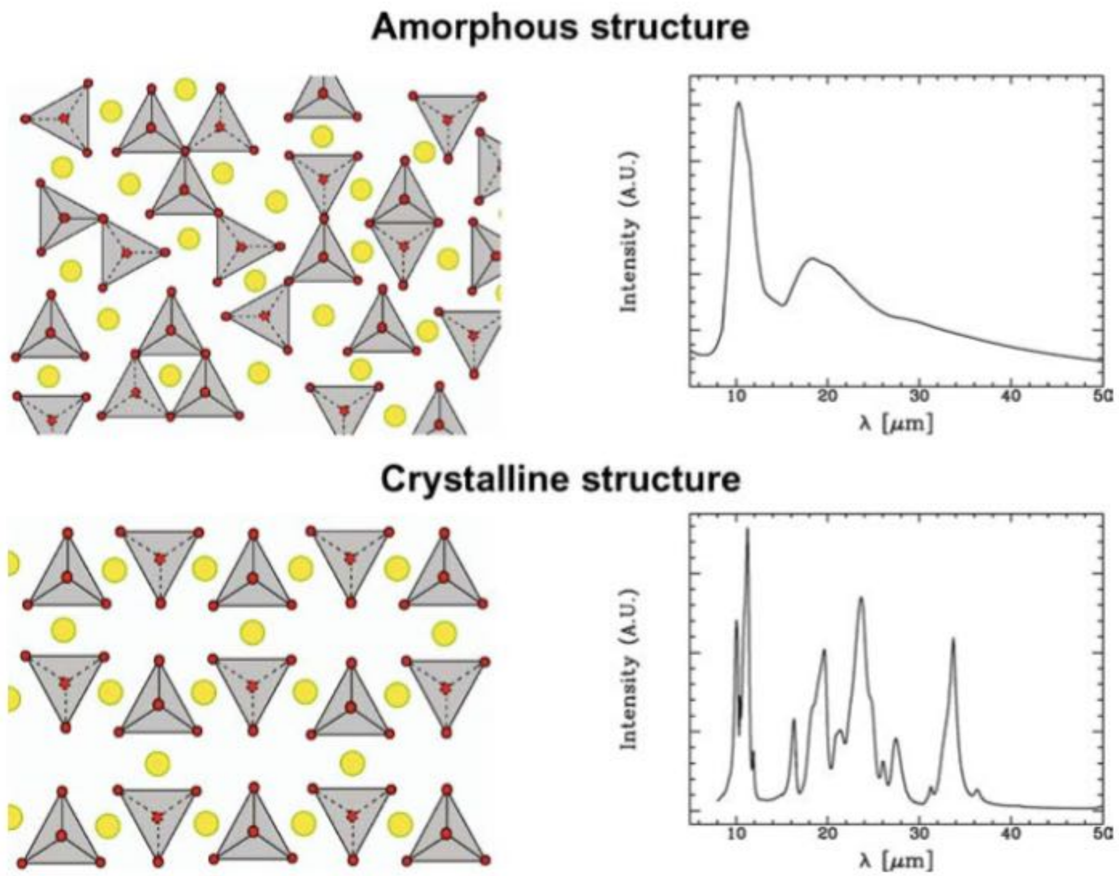

Credit: Molster, F., & Kemper, C. 2005, SSR, 119, 3

Absorption Coefficients

Affected by:

- Grain size
- Grain shape
- Mg/Fe content
- Temperature
- Laboratory conditions

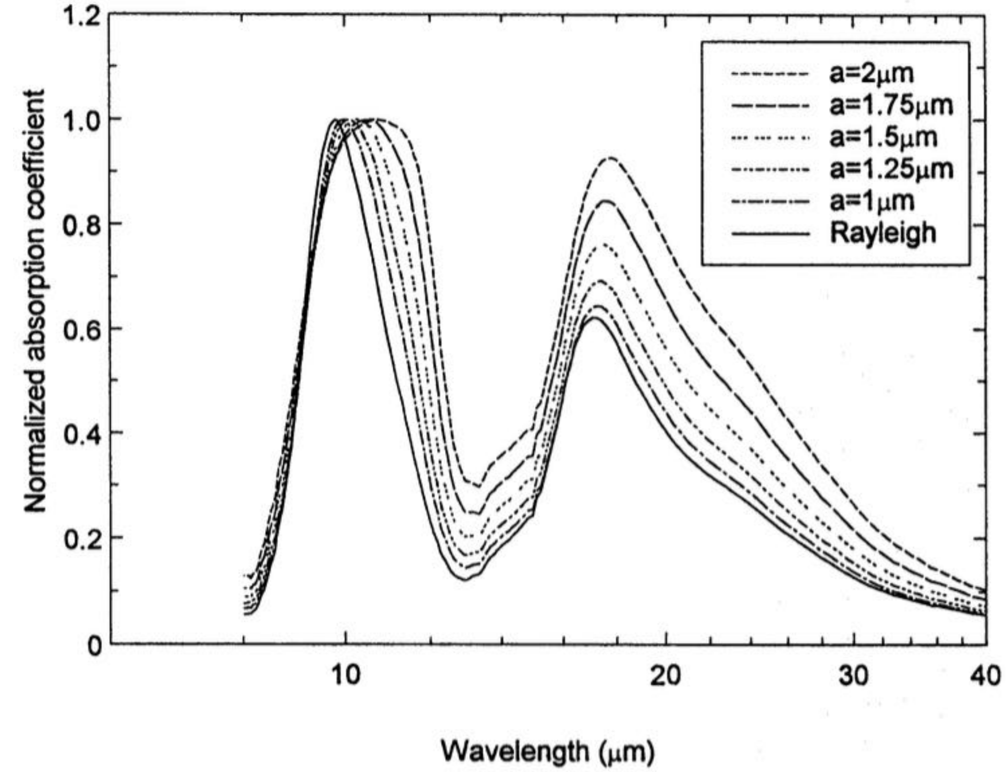

Credit: Dorschner, J., Begemann, B., Henning, T., Jaeger, C., & Mutschke, H. 1995, AAP, 300, 503

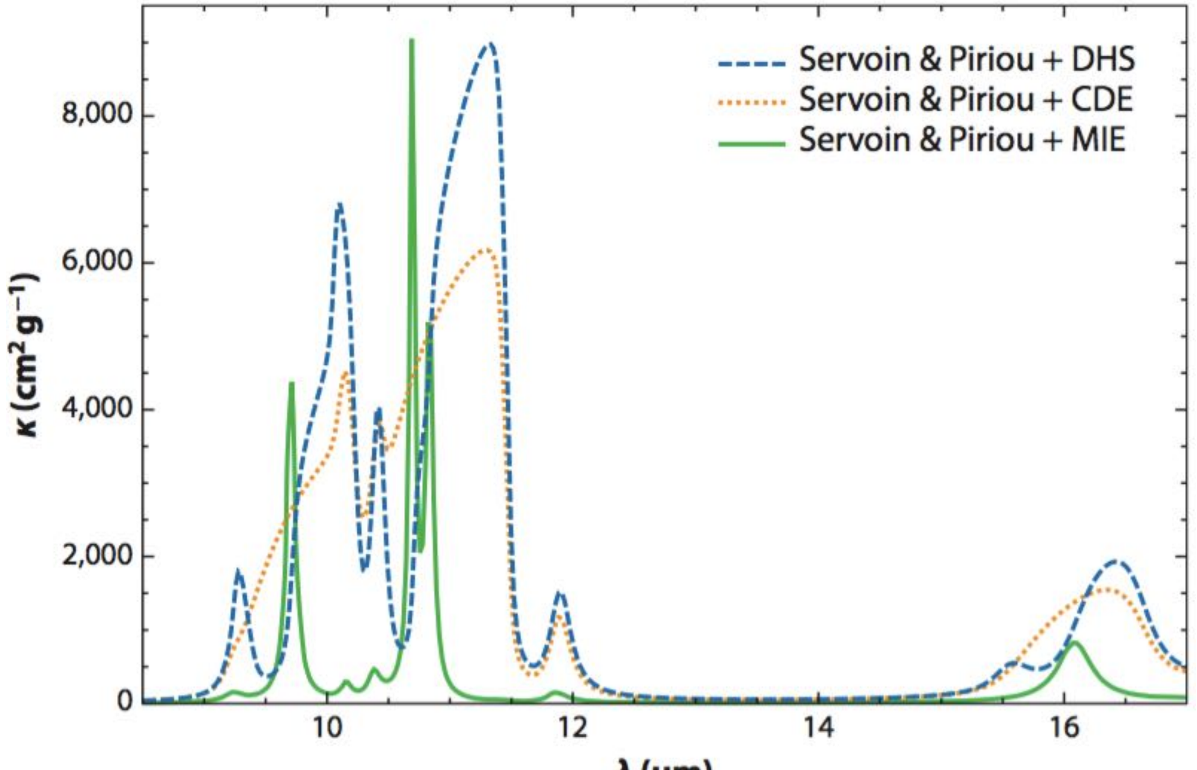

Credit: Henning, T. 2010, ARAA, 48, 21

Model

- Absorption coefficients were calculated using a homogeneous sphere approximation
- Two grain sizes of 0.1 μm (small) and 2.0 μm (large) were used
- Python module 'pymiecoated' was used to calculate the mass absorption coefficients for the 2.0 μm grains

Dust Species	Composition	Structure	Density (g/cm^3)	Grain Size (μm)	Reference
Forsterite	Mg_2SiO_4	C	3.27	0.1	Koike et al. (2003)
Olivine	Mg_2SiO_4	A	3.71	0.1, 2.0	Dorschner et al. (1995)
Pyroxene	$MgSiO_3$	A	3.20	0.1, 2.0	Dorschner et al. (1995)
Carbon	Pyrolized at 400° C	A	1.435	0.1, 2.0	Jaeger et al. (1998b)
Silicon Carbide	α-SiC	C	3.26	0.1, 2.0	Pegourie (1988)
Graphite		C	2.24	0.1, 2.0	Draine & Lee (1984)
Metallic Iron	Fe	C	7.87	0.1, 2.0	Pollack et al. (1994)

NOTE—The mineral structure is denoted as either amorphous (A) or crystalline (C).

Data

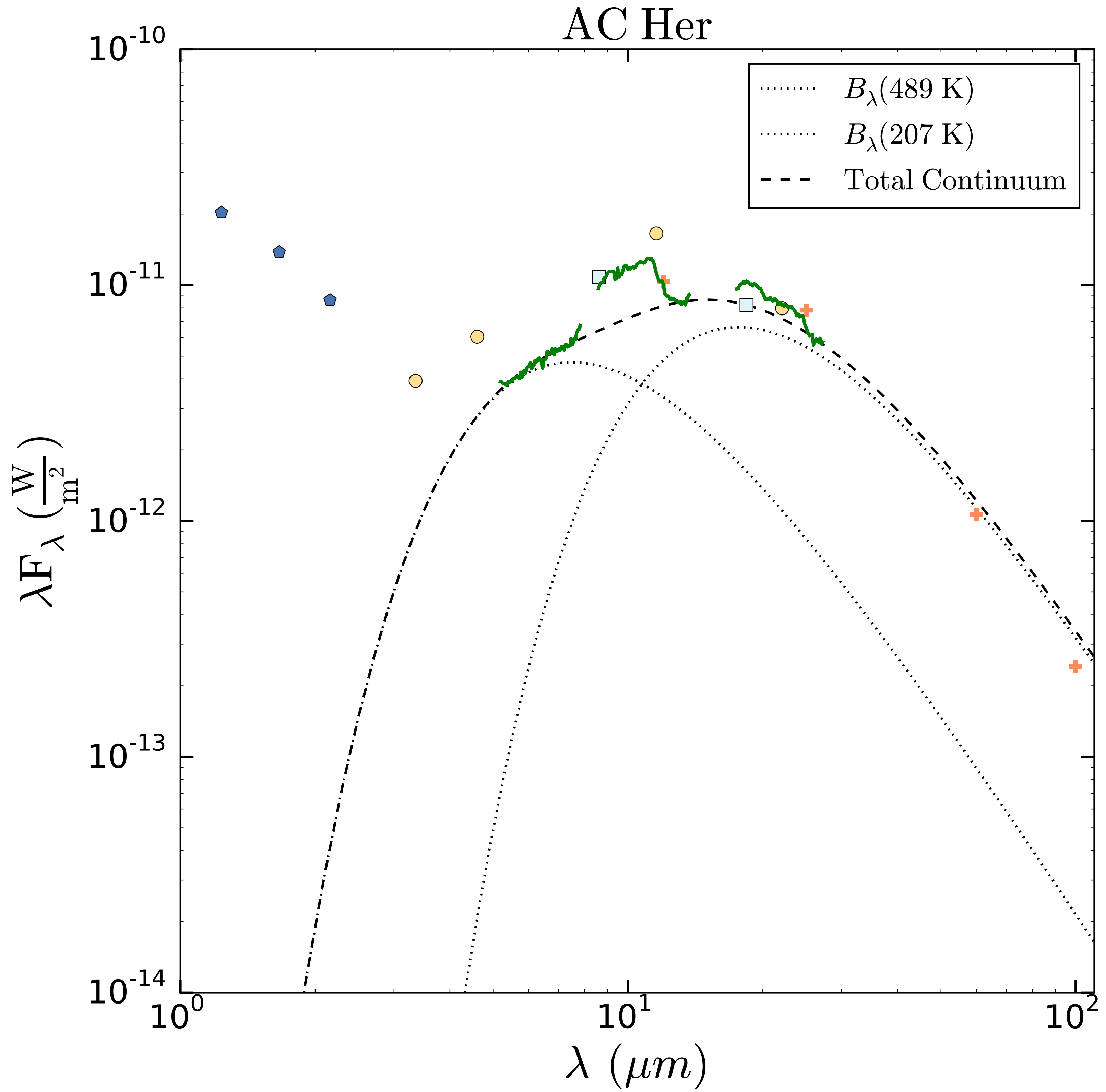

AC Her
$B_\lambda(489\ \mathrm{K})$
$B_\lambda(207\ \mathrm{K})$
Total Continuum
10^{-10}
10^{-11}
10^{-12}
10^{-13}
10^{-14}
$\lambda F_\lambda\ (\frac{W}{m^2})$
10^{0}
10^{1}
10^{2}
$\lambda\ (\mu m)$

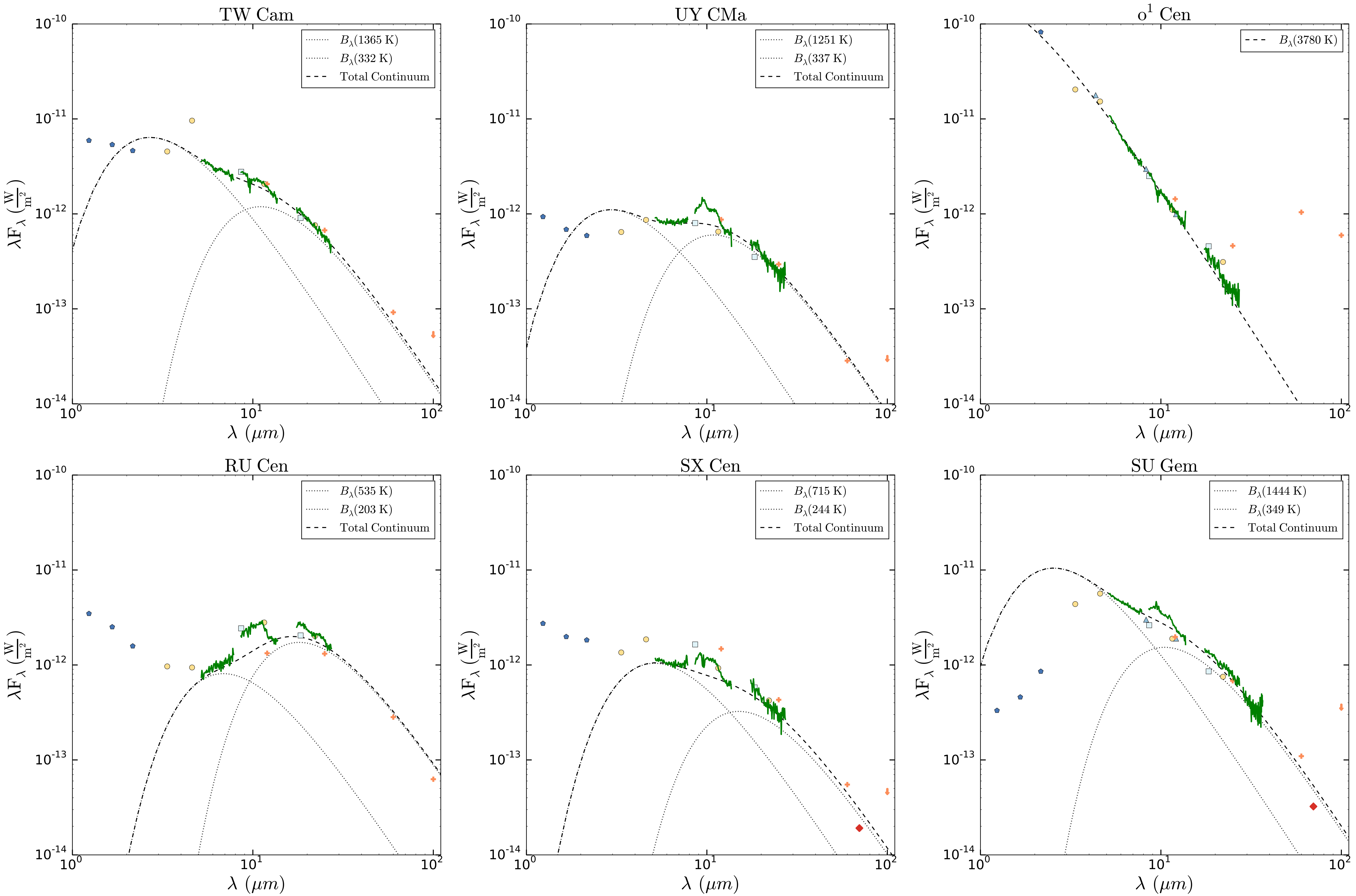
TW Cam
B_λ(1365 K)
B_λ(332 K)
Total Continuum
UY CMa
B_λ(1251 K)
B_λ(337 K)
Total Continuum
o^1 Cen
B_λ(3780 K)
RU Cen
B_λ(535 K)
B_λ(203 K)
Total Continuum
SX Cen
B_λ(715 K)
B_λ(244 K)
Total Continuum
SU Gem
B_λ(1444 K)
B_λ(349 K)
Total Continuum
$\lambda F_\lambda \left(\frac{W}{m^2}\right)$
λ (μm)
10^{-10}
10^{-11}
10^{-12}
10^{-13}
10^{-14}
10^{0}
10^{1}
10^{2}

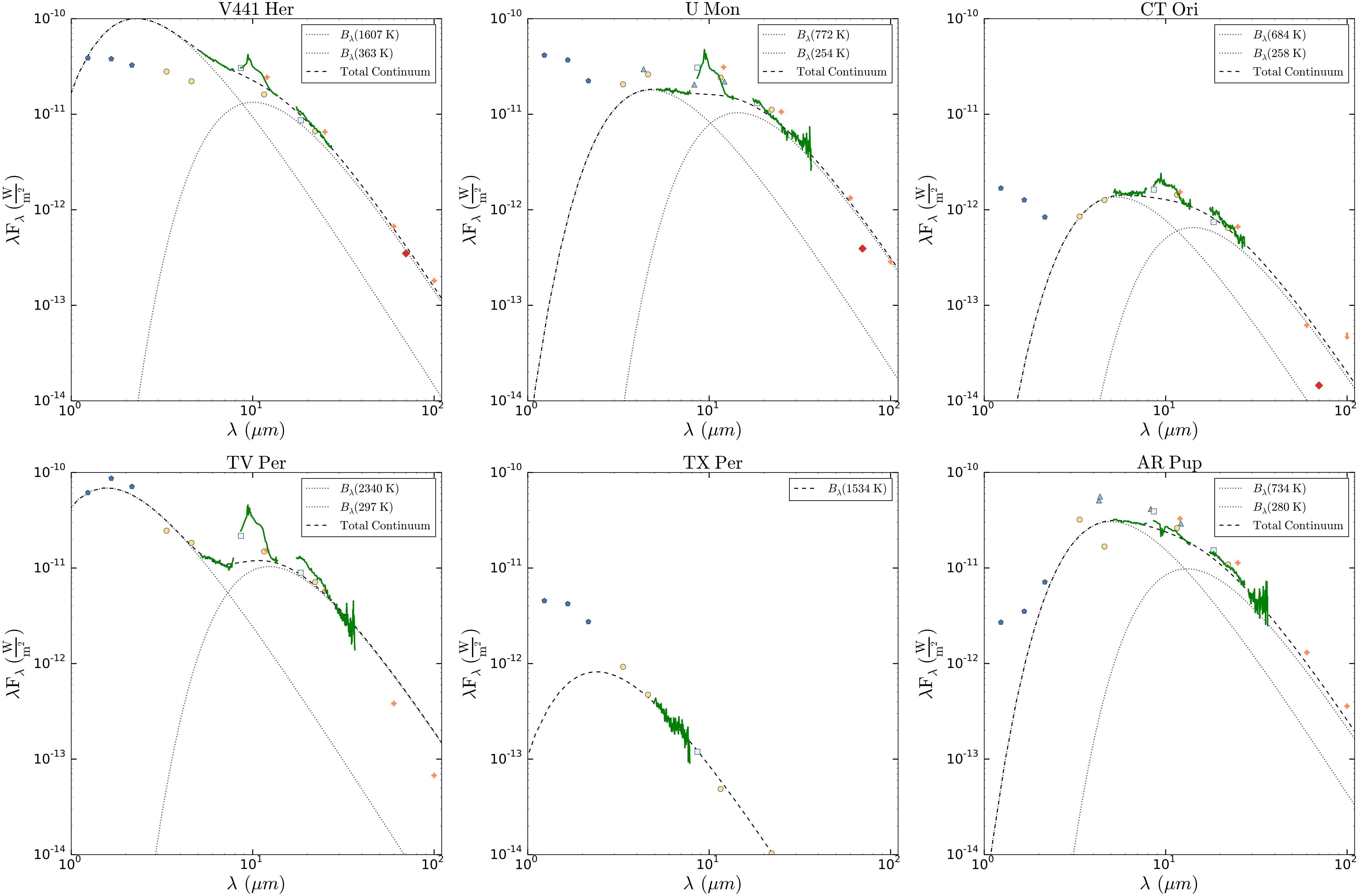

V441 Her
B_λ(1607 K)
B_λ(363 K)
Total Continuum
U Mon
B_λ(772 K)
B_λ(254 K)
Total Continuum
CT Ori
B_λ(684 K)
B_λ(258 K)
Total Continuum
TV Per
B_λ(2340 K)
B_λ(297 K)
Total Continuum
TX Per
B_λ(1534 K)
AR Pup
B_λ(734 K)
B_λ(280 K)
Total Continuum
$\lambda F_\lambda (\frac{W}{m^2})$
$\lambda\ (\mu m)$
10^{-10}
10^{-11}
10^{-12}
10^{-13}
10^{-14}
10^0
10^1
10^2

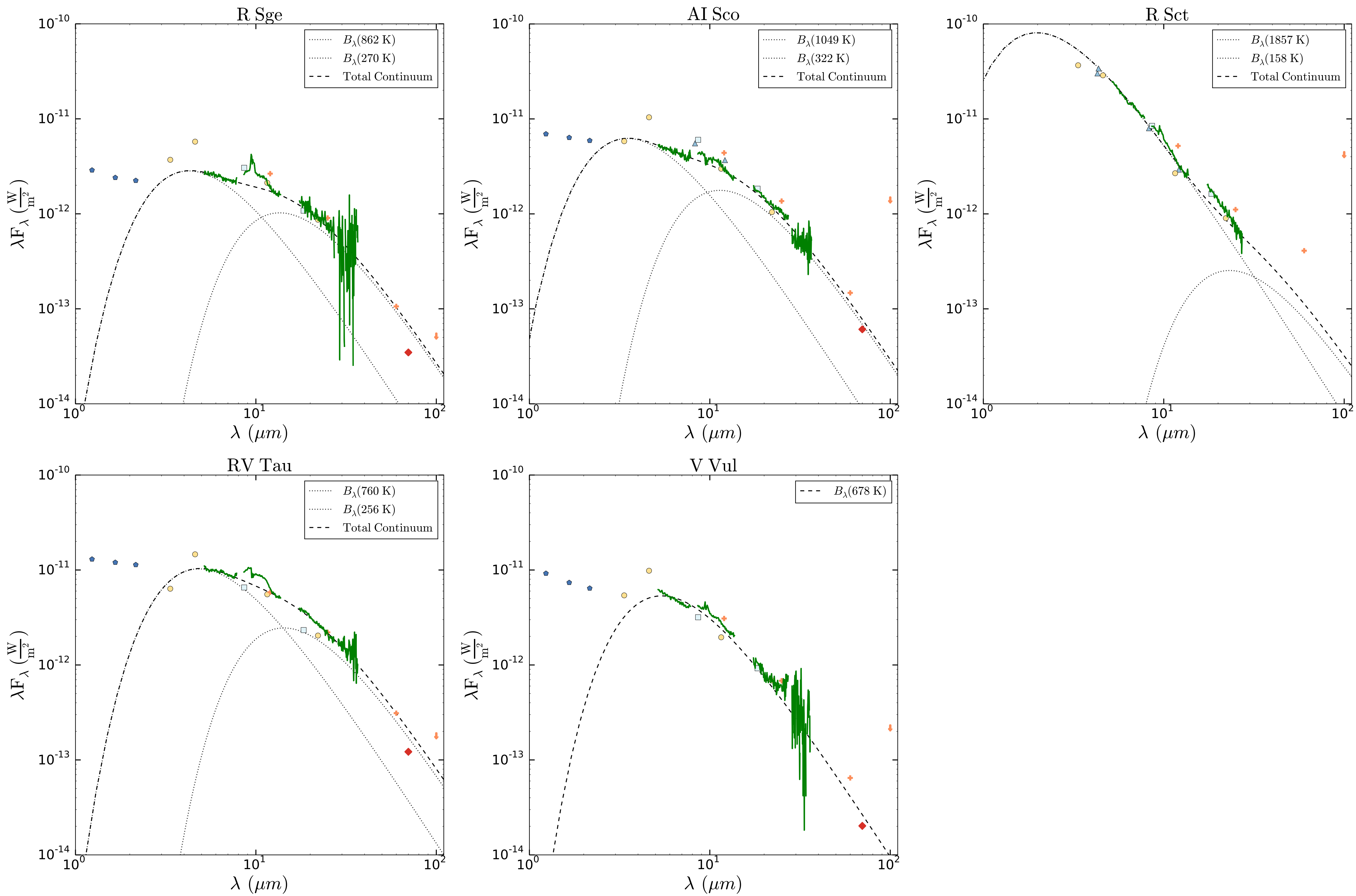

R Sge
B_λ(862 K)
B_λ(270 K)
Total Continuum
AI Sco
B_λ(1049 K)
B_λ(322 K)
Total Continuum
R Sct
B_λ(1857 K)
B_λ(158 K)
Total Continuum
RV Tau
B_λ(760 K)
B_λ(256 K)
Total Continuum
V Vul
B_λ(678 K)
$\lambda F_\lambda\,(\frac{W}{m^2})$
$\lambda\ (\mu m)$
10^{-10}
10^{-11}
10^{-12}
10^{-13}
10^{-14}
10^{0}
10^{1}
10^{2}

Results

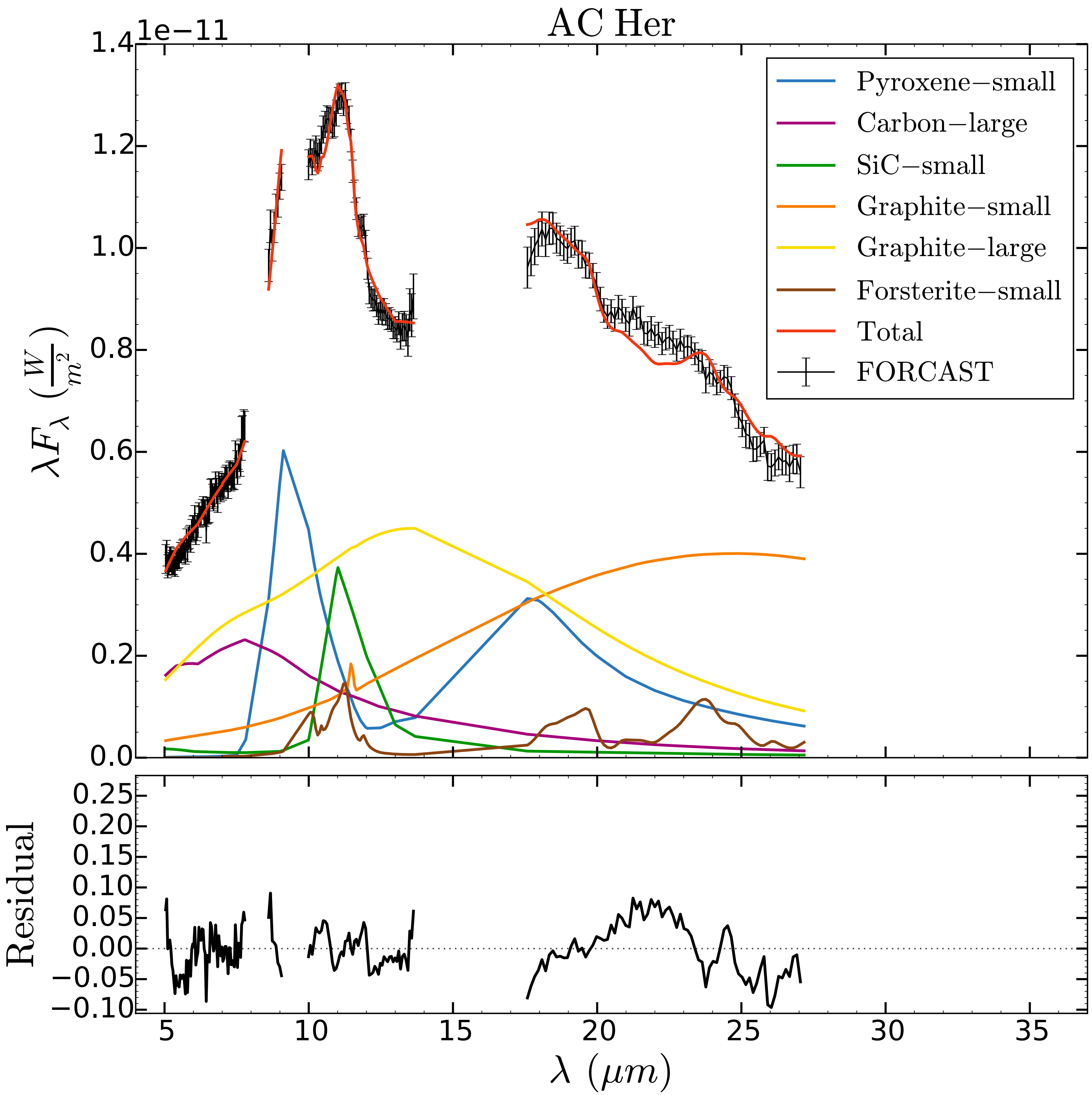

AC Her
1e−11
1.4
1.2
1.0
0.8
0.6
0.4
0.2
0.0
$\lambda F_\lambda\ (\frac{W}{m^2})$
Pyroxene−small
Carbon−large
SiC−small
Graphite−small
Graphite−large
Forsterite−small
Total
FORCAST
Residual
0.25
0.20
0.15
0.10
0.05
0.00
−0.05
−0.10
5
10
15
20
25
30
35
$\lambda\ (\mu m)$

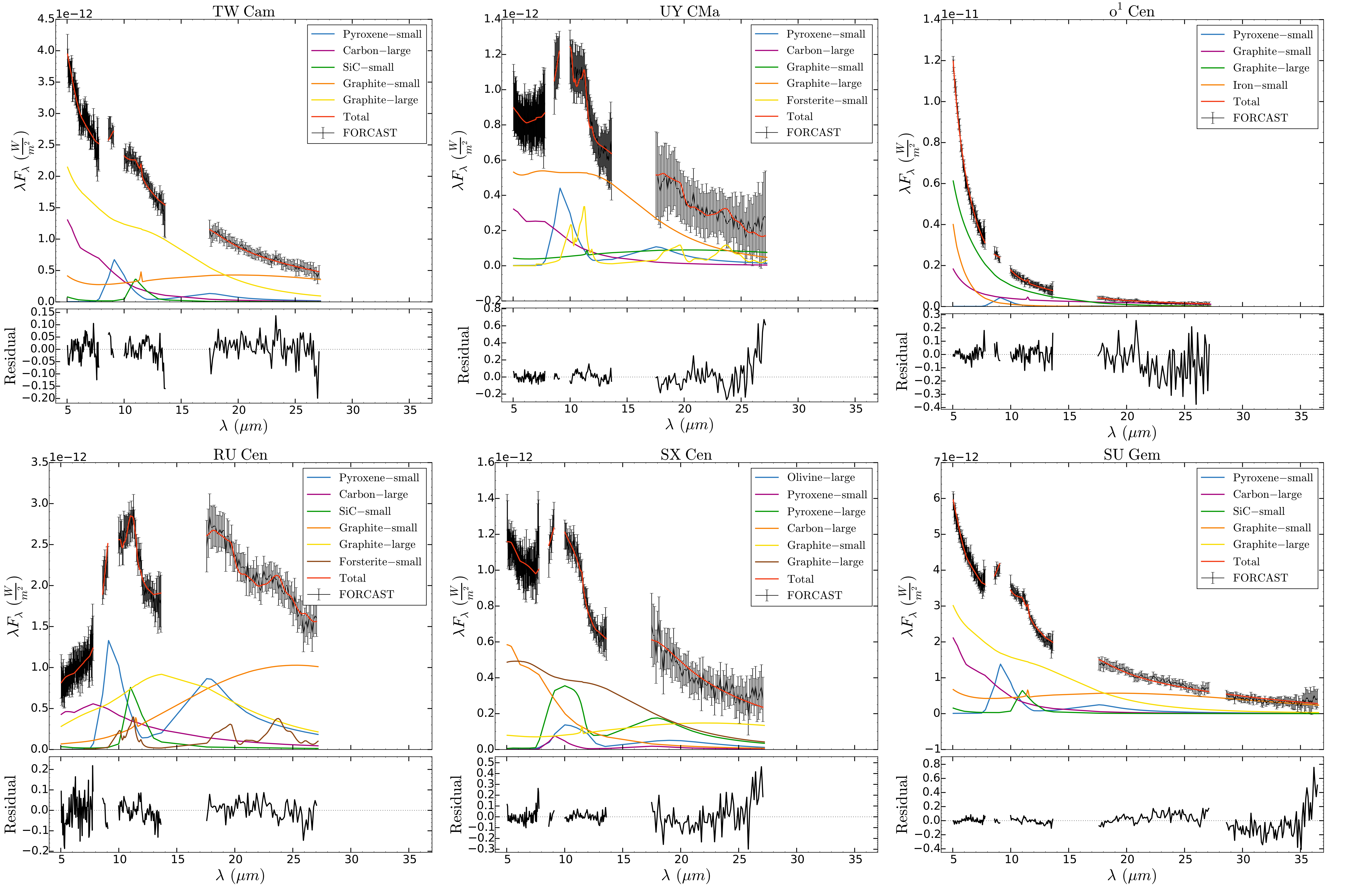
TW Cam
Pyroxene−small
Carbon−large
SiC−small
Graphite−small
Graphite−large
Total
FORCAST
UY CMa
Pyroxene−small
Carbon−large
Graphite−small
Graphite−large
Forsterite−small
Total
FORCAST
o1 Cen
Pyroxene−small
Graphite−small
Graphite−large
Iron−small
Total
FORCAST
RU Cen
Pyroxene−small
Carbon−large
SiC−small
Graphite−small
Graphite−large
Forsterite−small
Total
FORCAST
SX Cen
Olivine−large
Pyroxene−small
Pyroxene−large
Carbon−large
Graphite−small
Graphite−large
Total
FORCAST
SU Gem
Pyroxene−small
Carbon−large
SiC−small
Graphite−small
Graphite−large
Total
FORCAST
λFλ (W/m²)
Residual
λ (μm)

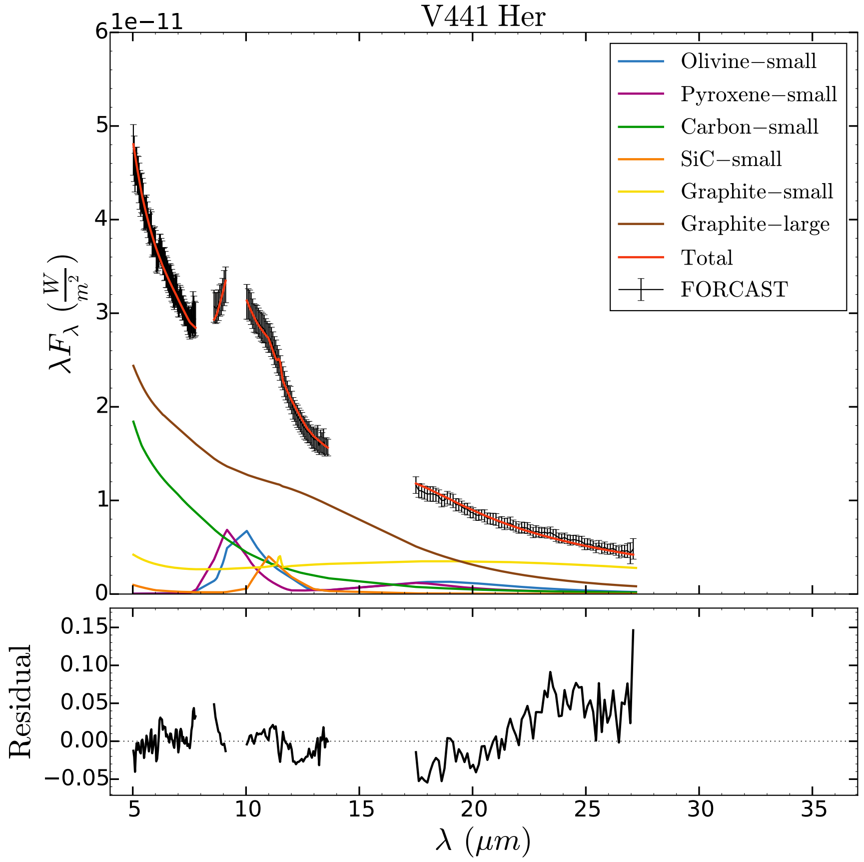
V441 Her
Olivine−small
Pyroxene−small
Carbon−small
SiC−small
Graphite−small
Graphite−large
Total
FORCAST
Residual
λ (μm)

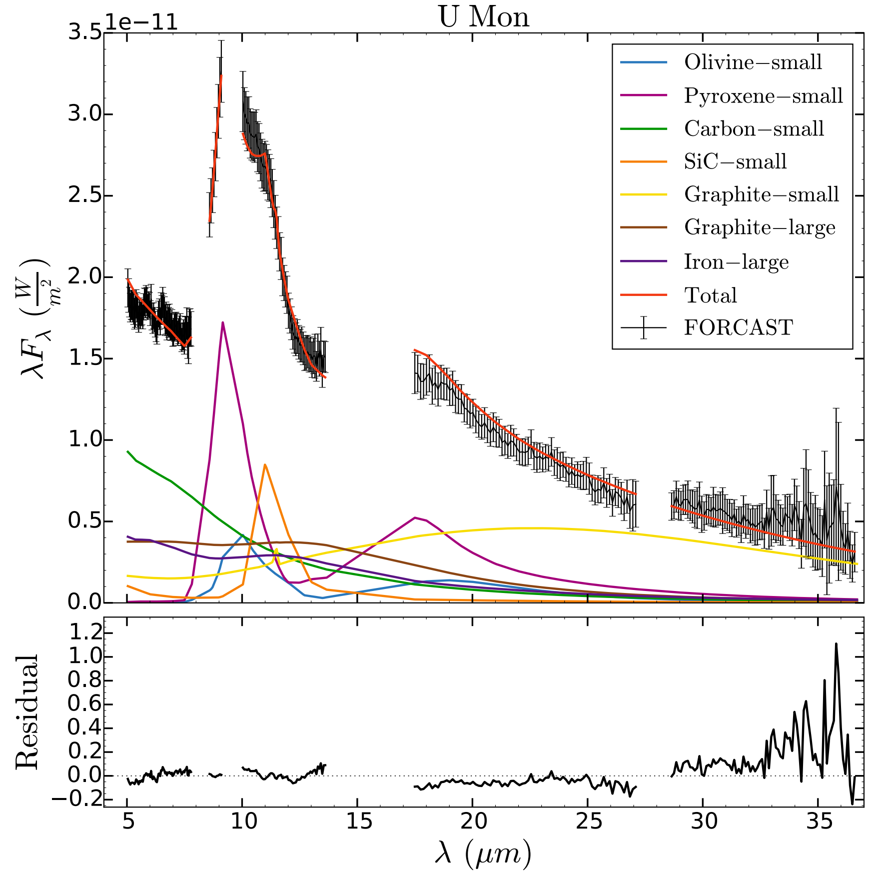
U Mon
Olivine−small
Pyroxene−small
Carbon−small
SiC−small
Graphite−small
Graphite−large
Iron−large
Total
FORCAST
Residual
λ (μm)

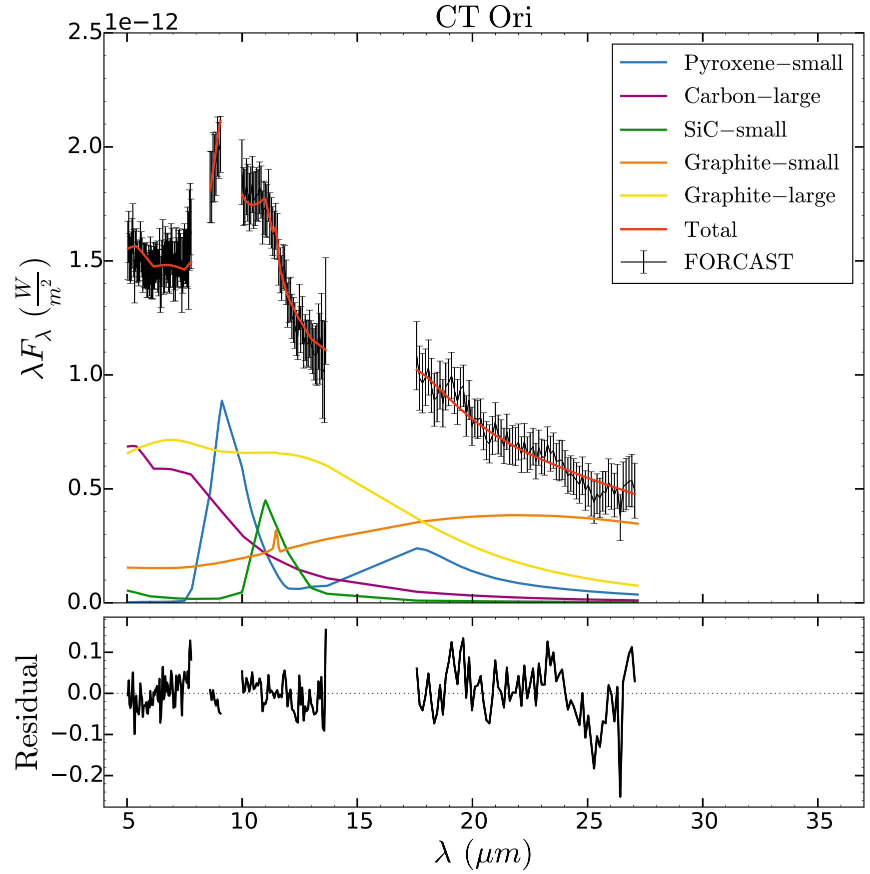
CT Ori
Pyroxene−small
Carbon−large
SiC−small
Graphite−small
Graphite−large
Total
FORCAST
Residual
λ (μm)

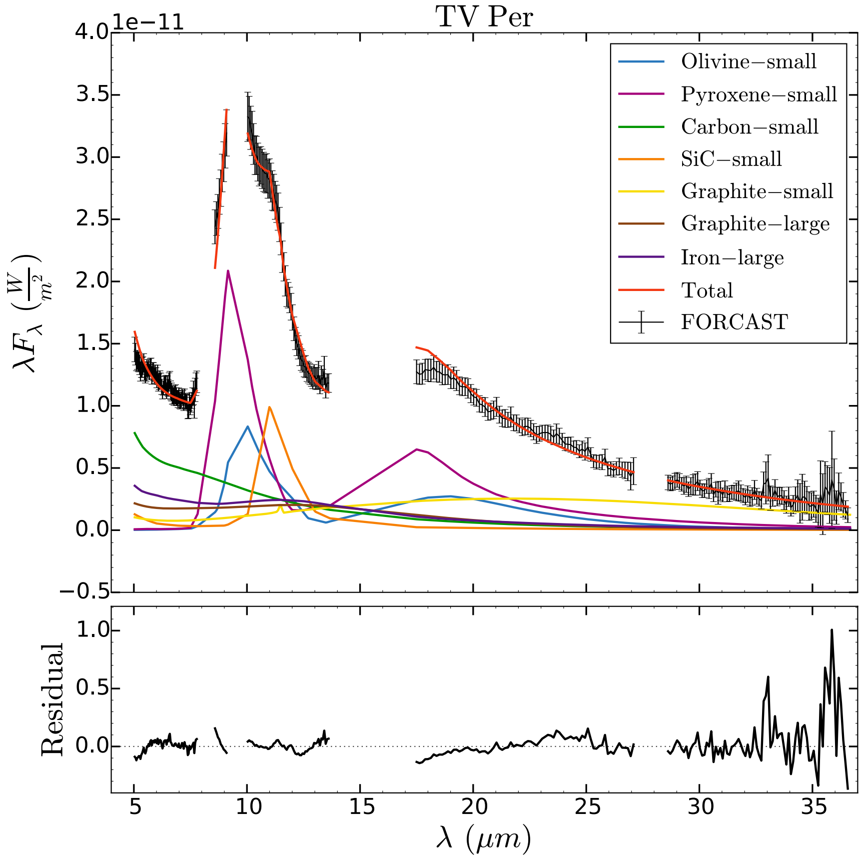
TV Per
Olivine−small
Pyroxene−small
Carbon−small
SiC−small
Graphite−small
Graphite−large
Iron−large
Total
FORCAST
Residual
λ (μm)

TX Per

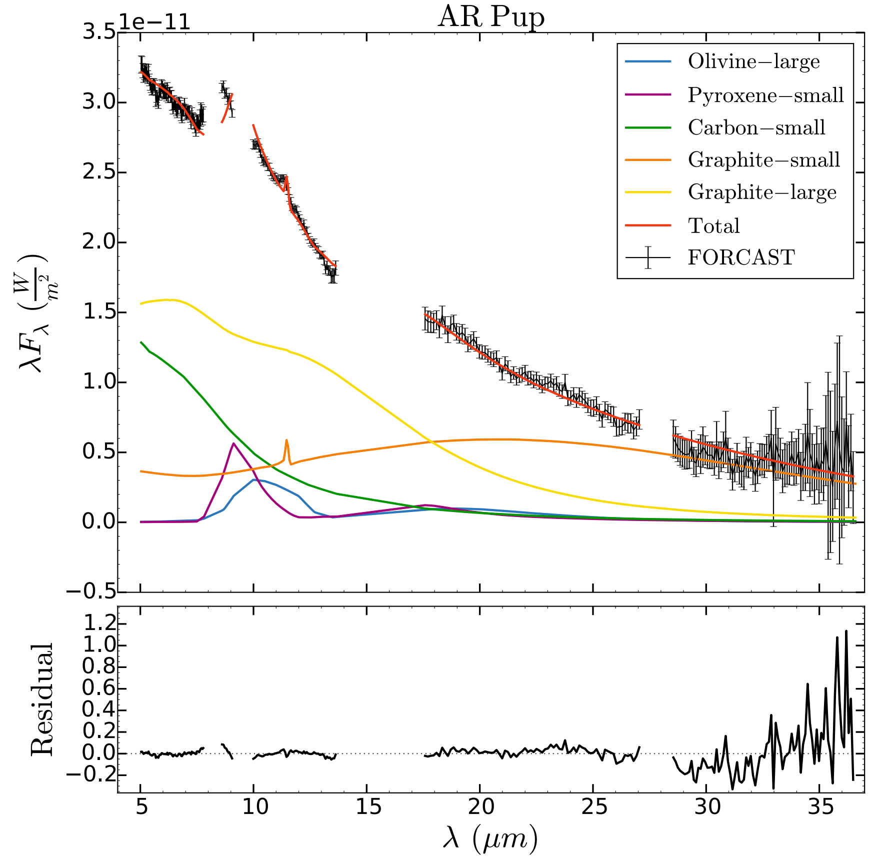
AR Pup
Olivine−large
Pyroxene−small
Carbon−small
Graphite−small
Graphite−large
Total
FORCAST
Residual
λ (μm)

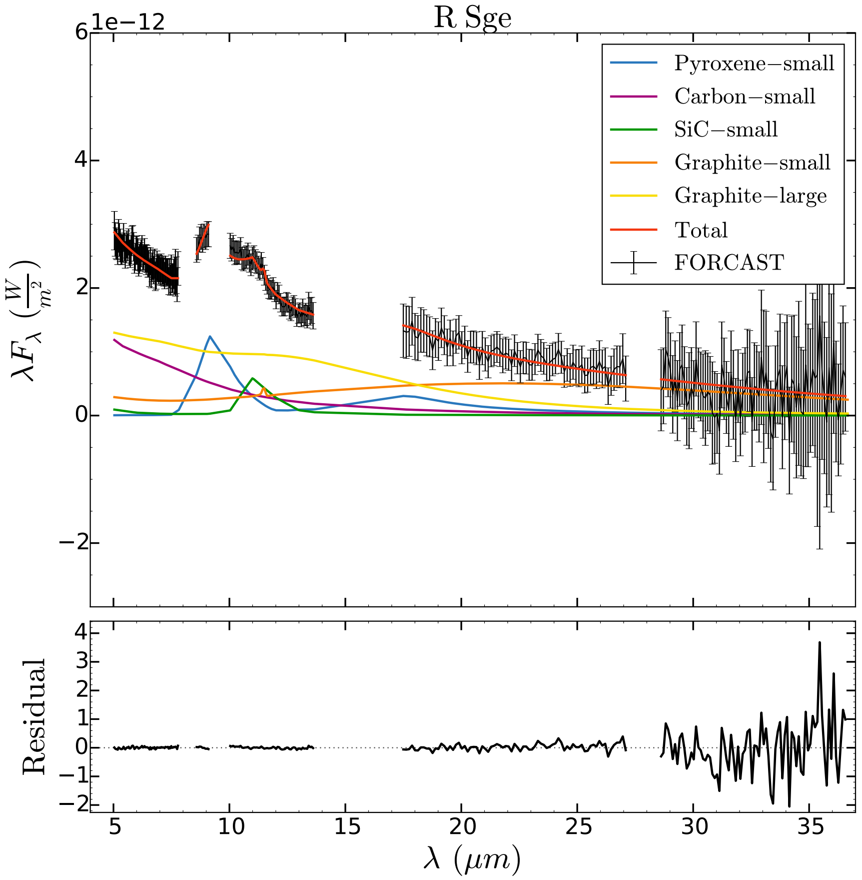
R Sge
1e−12
Pyroxene−small
Carbon−small
SiC−small
Graphite−small
Graphite−large
Total
FORCAST
$\lambda F_\lambda\ (\frac{W}{m^2})$
Residual
$\lambda\ (\mu m)$

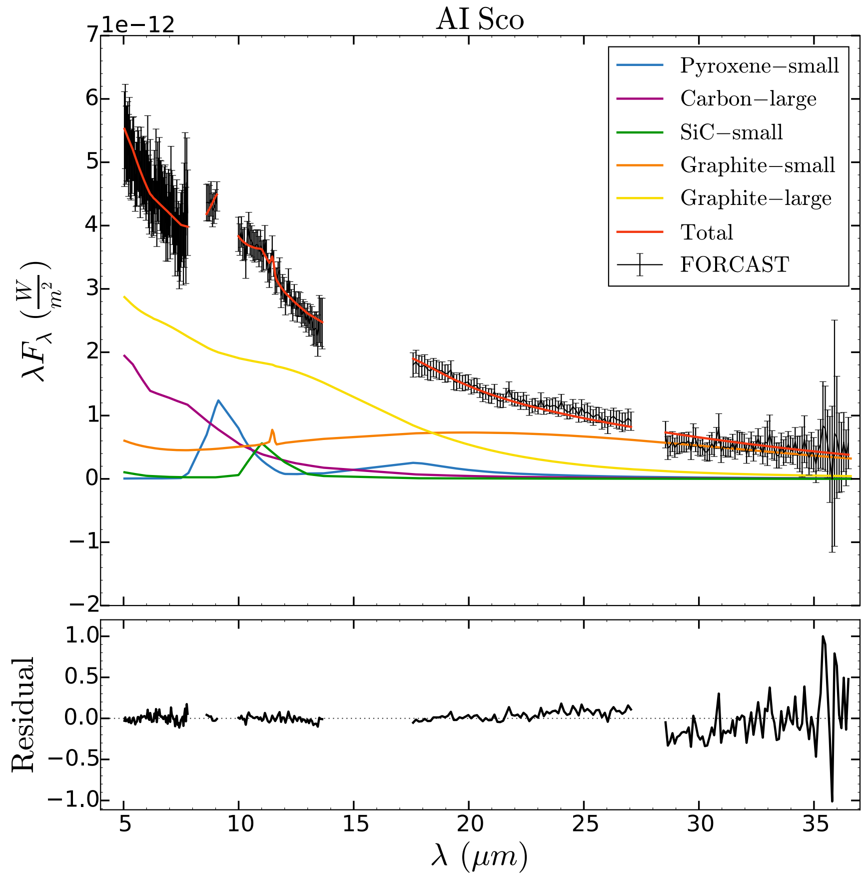
AI Sco
1e−12
Pyroxene−small
Carbon−large
SiC−small
Graphite−small
Graphite−large
Total
FORCAST
$\lambda F_\lambda\ (\frac{W}{m^2})$
Residual
$\lambda\ (\mu m)$

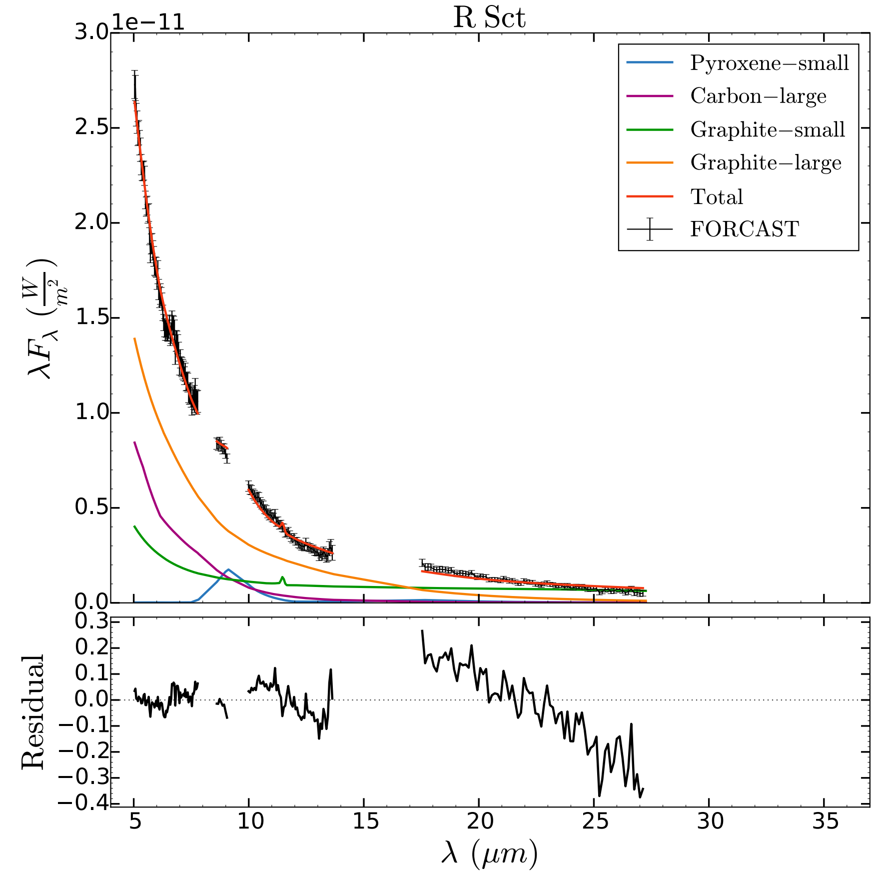
R Sct
1e−11
Pyroxene−small
Carbon−large
Graphite−small
Graphite−large
Total
FORCAST
$\lambda F_\lambda\ (\frac{W}{m^2})$
Residual
$\lambda\ (\mu m)$

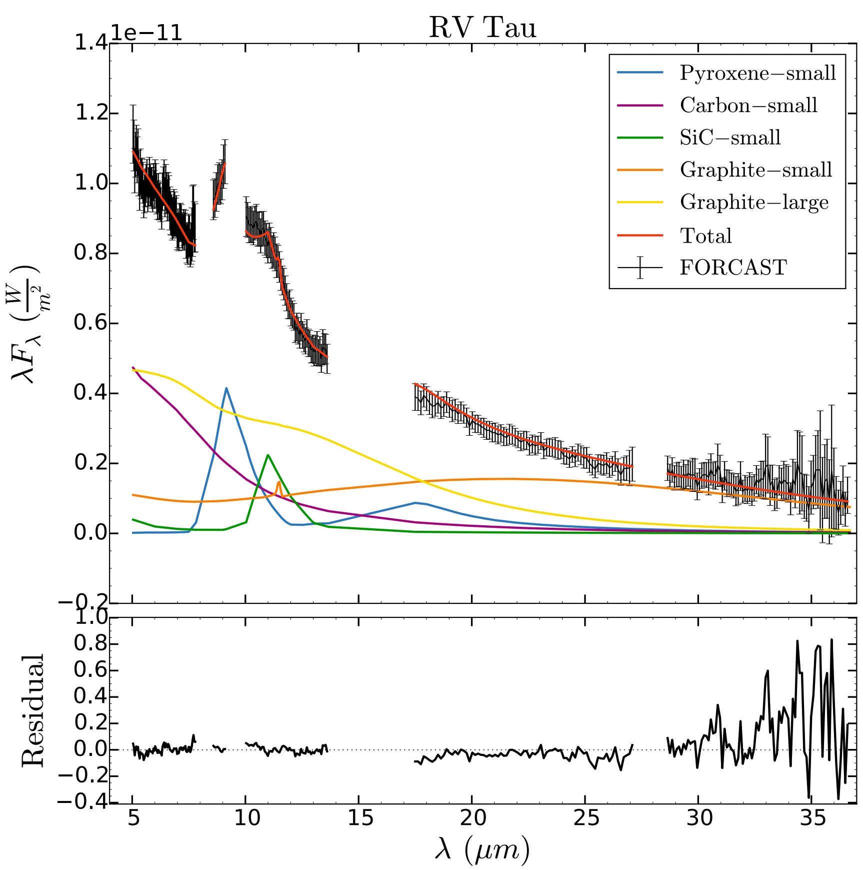
RV Tau
1e−11
Pyroxene−small
Carbon−small
SiC−small
Graphite−small
Graphite−large
Total
FORCAST
$\lambda F_\lambda\ (\frac{W}{m^2})$
Residual
$\lambda\ (\mu m)$

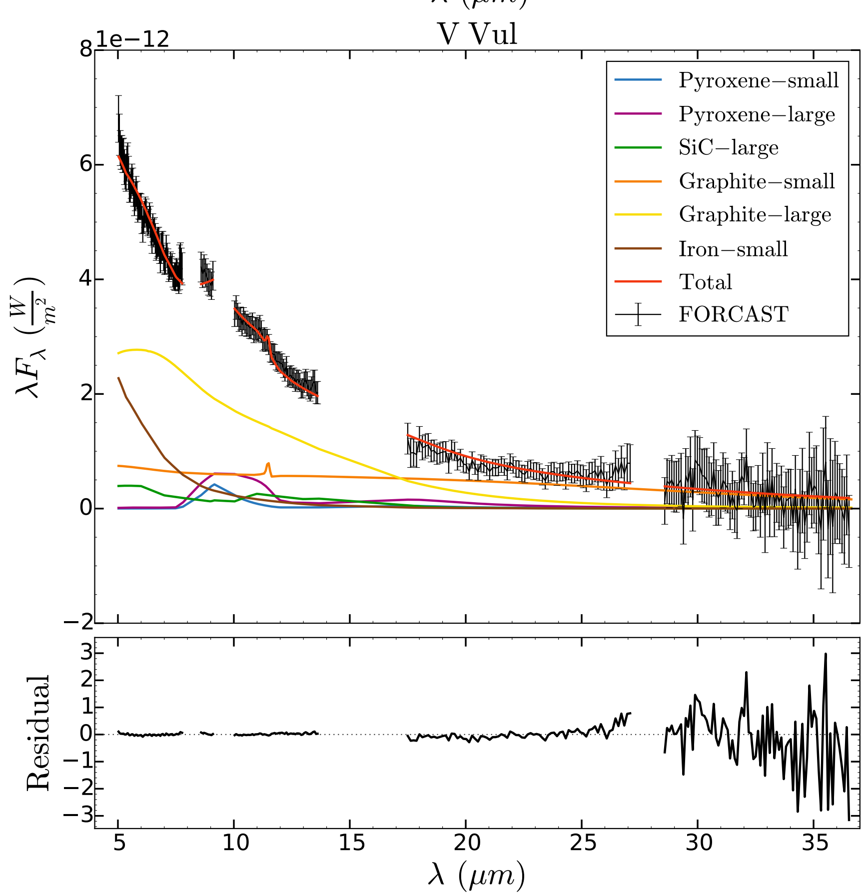
V Vul
1e−12
Pyroxene−small
Pyroxene−large
SiC−large
Graphite−small
Graphite−large
Iron−small
Total
FORCAST
$\lambda F_\lambda\ (\frac{W}{m^2})$
Residual
$\lambda\ (\mu m)$

Model Covariance

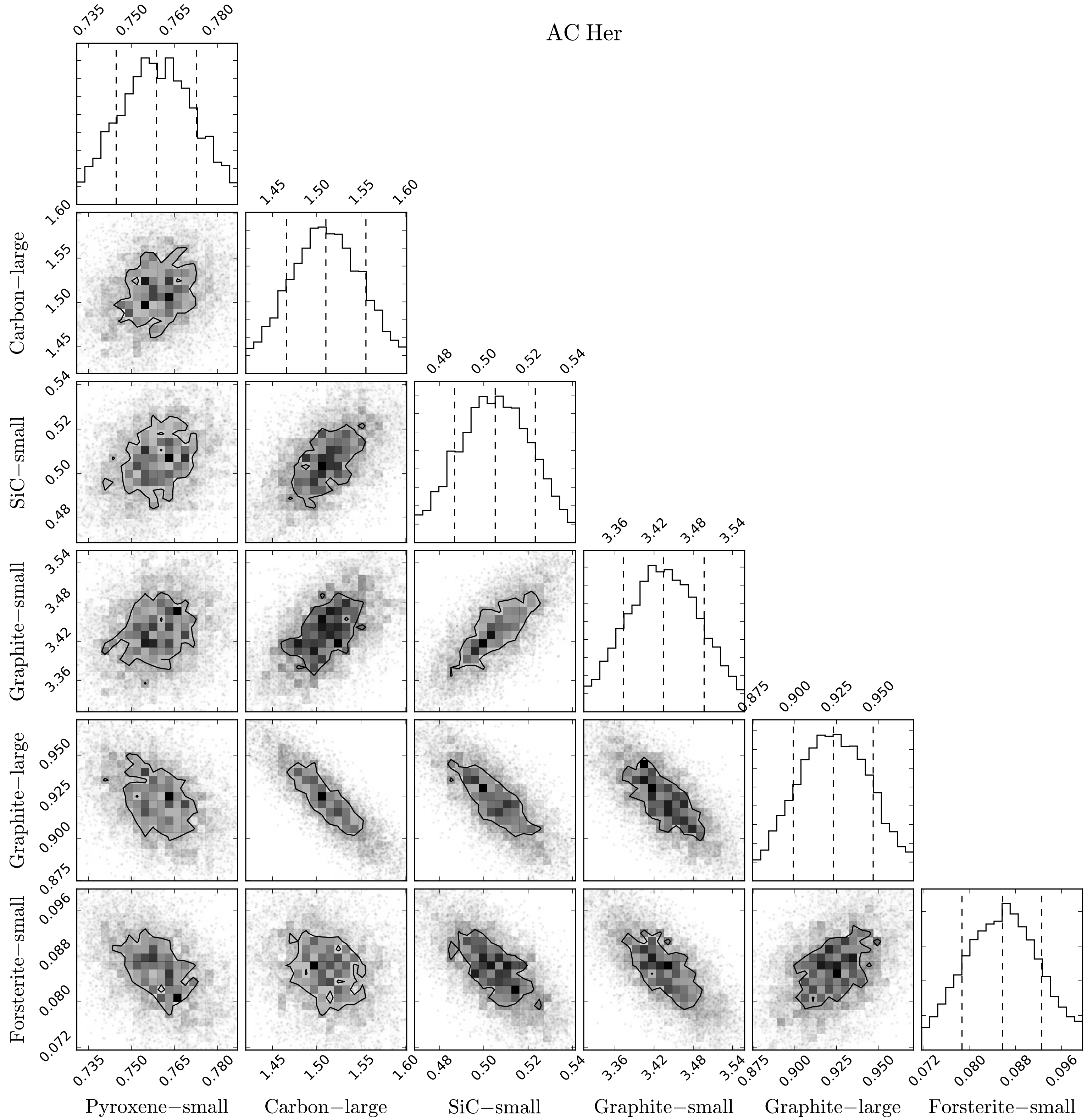

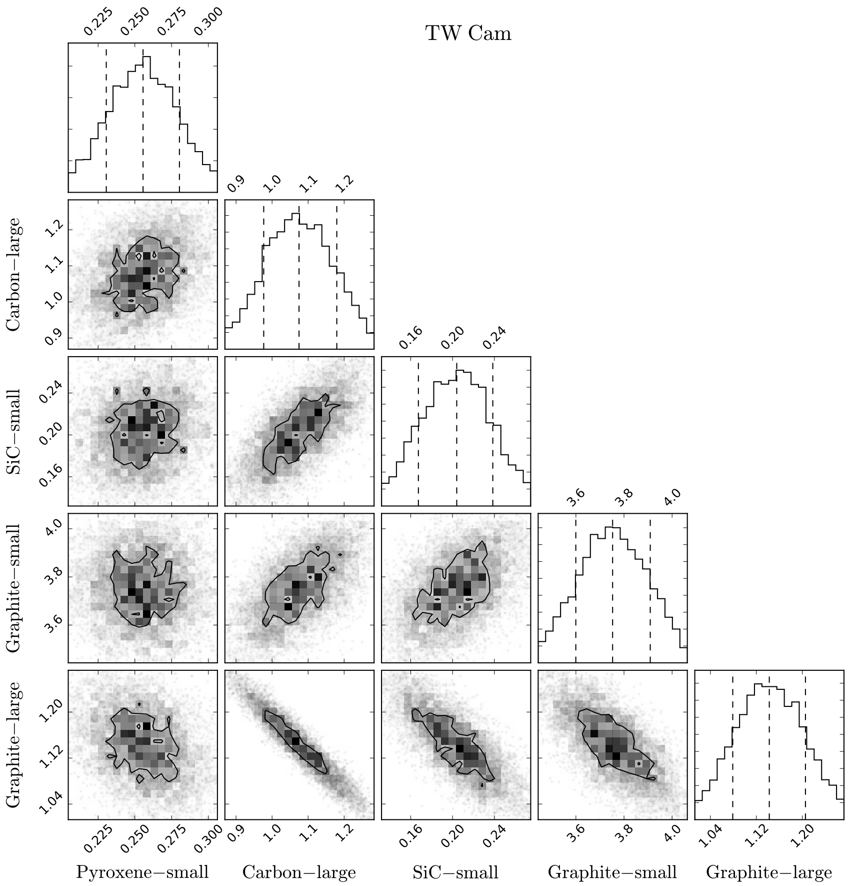
TW Cam
Carbon−large
SiC−small
Graphite−small
Graphite−large
Pyroxene−small
Carbon−large
SiC−small
Graphite−small
Graphite−large

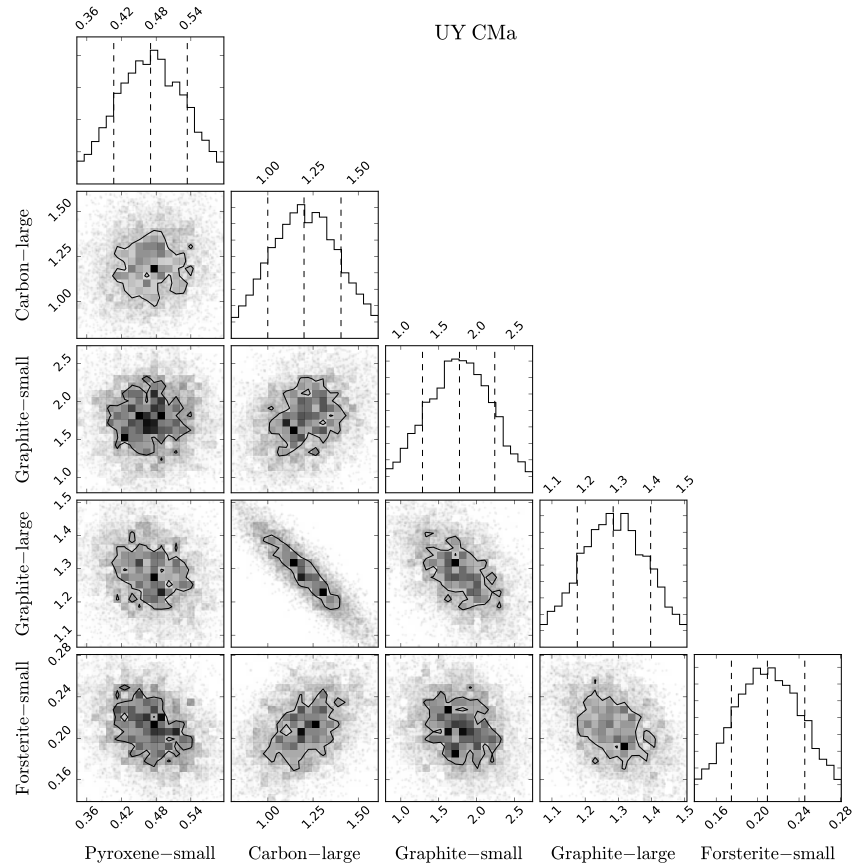
UY CMa
Carbon−large
Graphite−small
Graphite−large
Forsterite−small
Pyroxene−small
Carbon−large
Graphite−small
Graphite−large
Forsterite−small

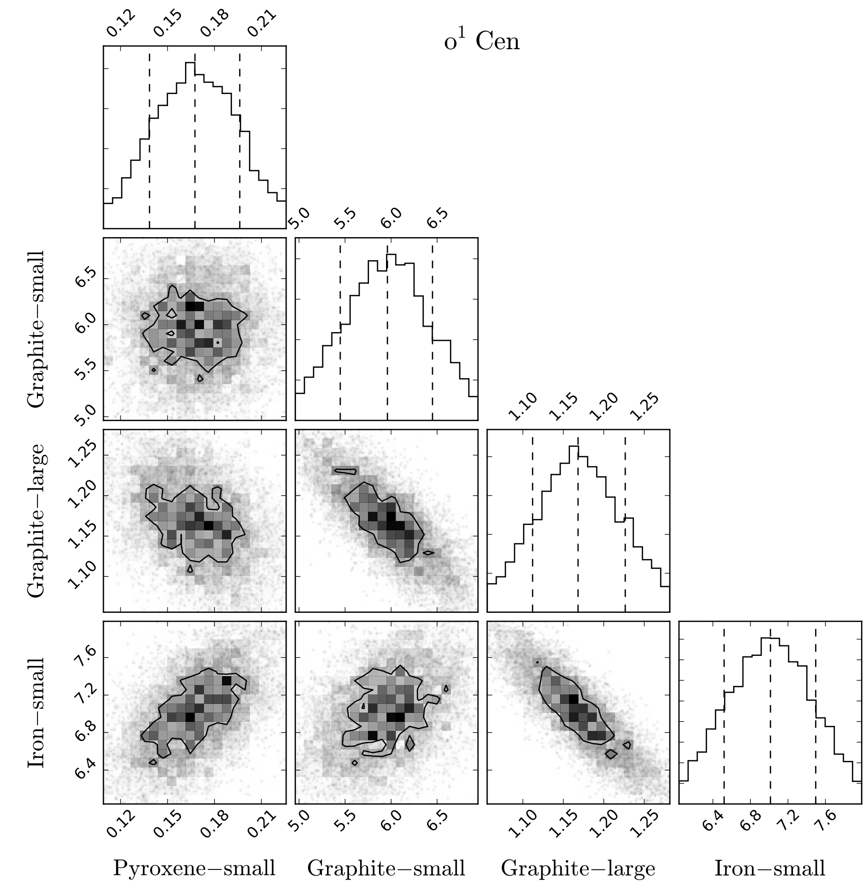
o1 Cen
Graphite−small
Graphite−large
Iron−small
Pyroxene−small
Graphite−small
Graphite−large
Iron−small

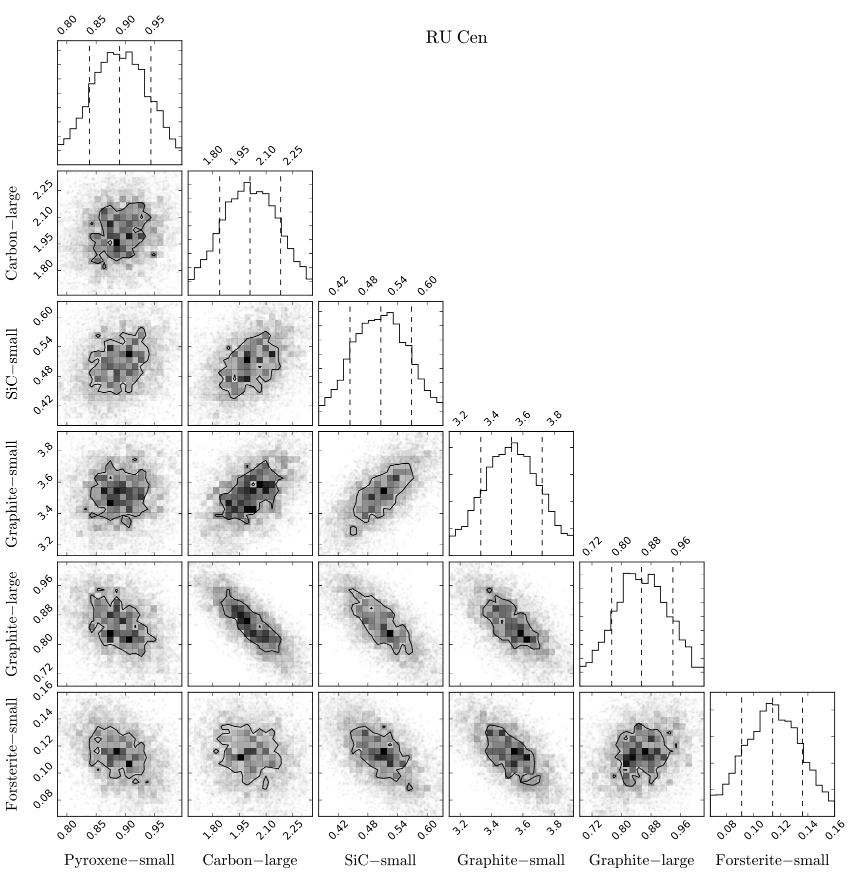
RU Cen
Carbon−large
SiC−small
Graphite−small
Graphite−large
Forsterite−small
Pyroxene−small
Carbon−large
SiC−small
Graphite−small
Graphite−large
Forsterite−small

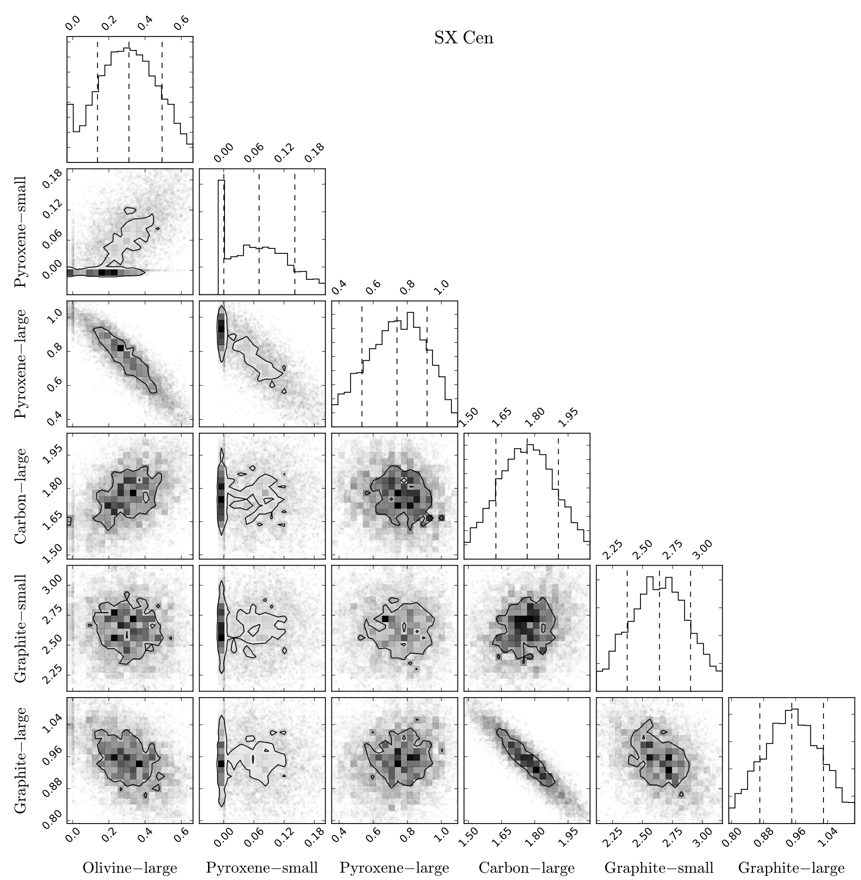
SX Cen
Pyroxene−small
Pyroxene−large
Carbon−large
Graphite−small
Graphite−large
Olivine−large
Pyroxene−small
Pyroxene−large
Carbon−large
Graphite−small
Graphite−large

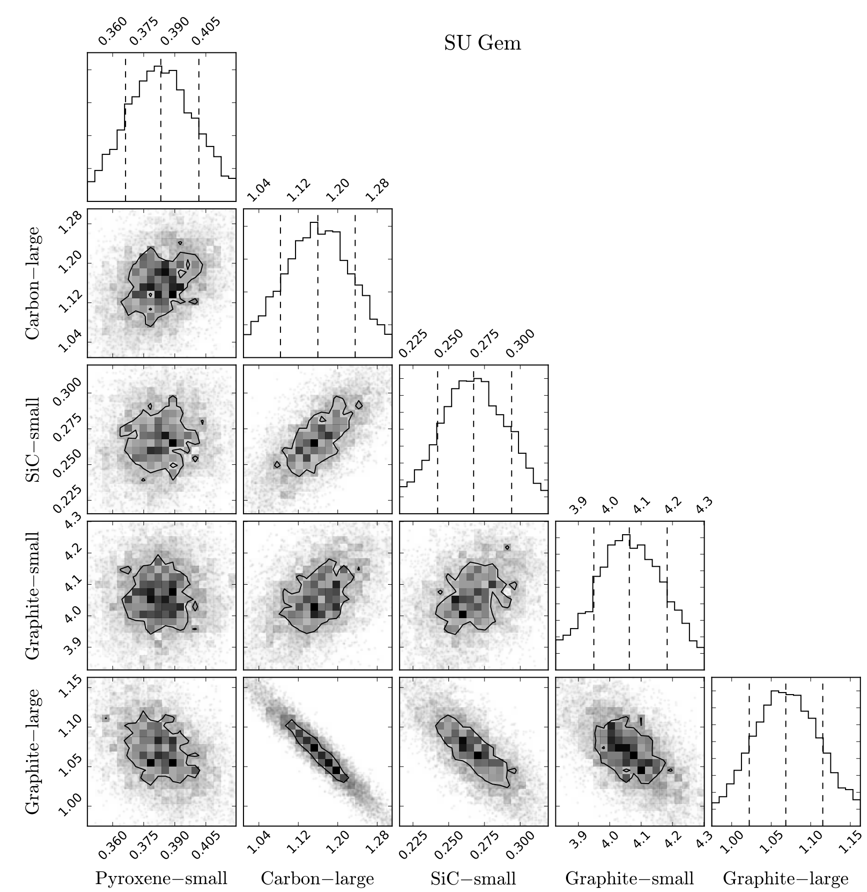
SU Gem
Carbon−large
SiC−small
Graphite−small
Graphite−large
Pyroxene−small
Carbon−large
SiC−small
Graphite−small
Graphite−large

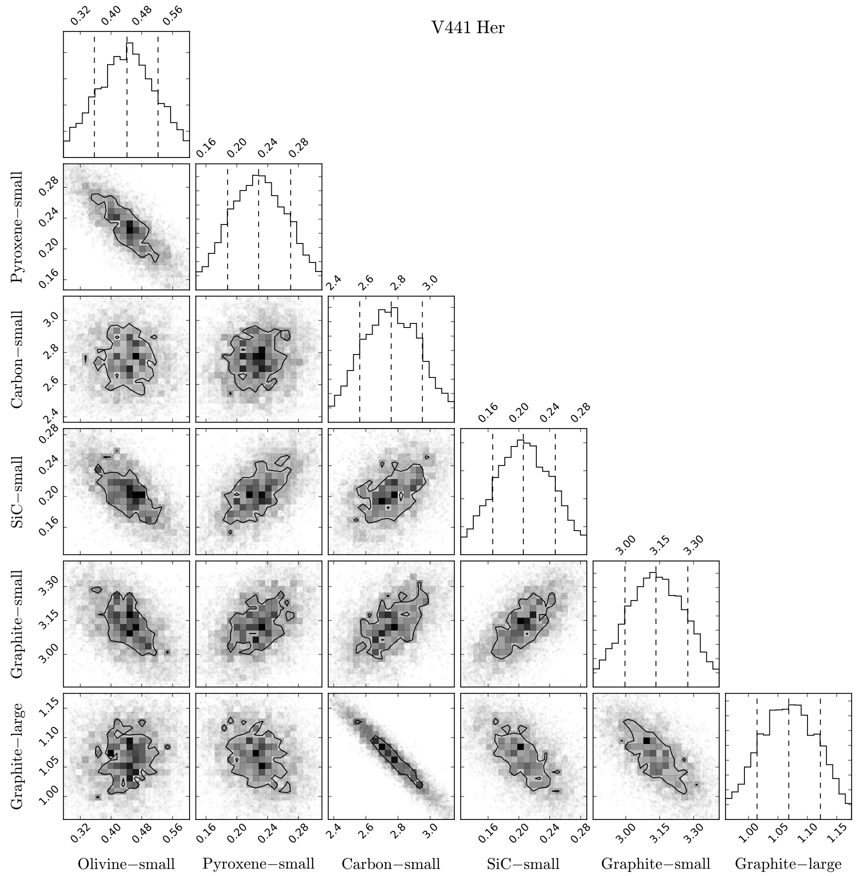
V441 Her
Pyroxene−small
Carbon−small
SiC−small
Graphite−small
Graphite−large
Olivine−small
Pyroxene−small
Carbon−small
SiC−small
Graphite−small
Graphite−large

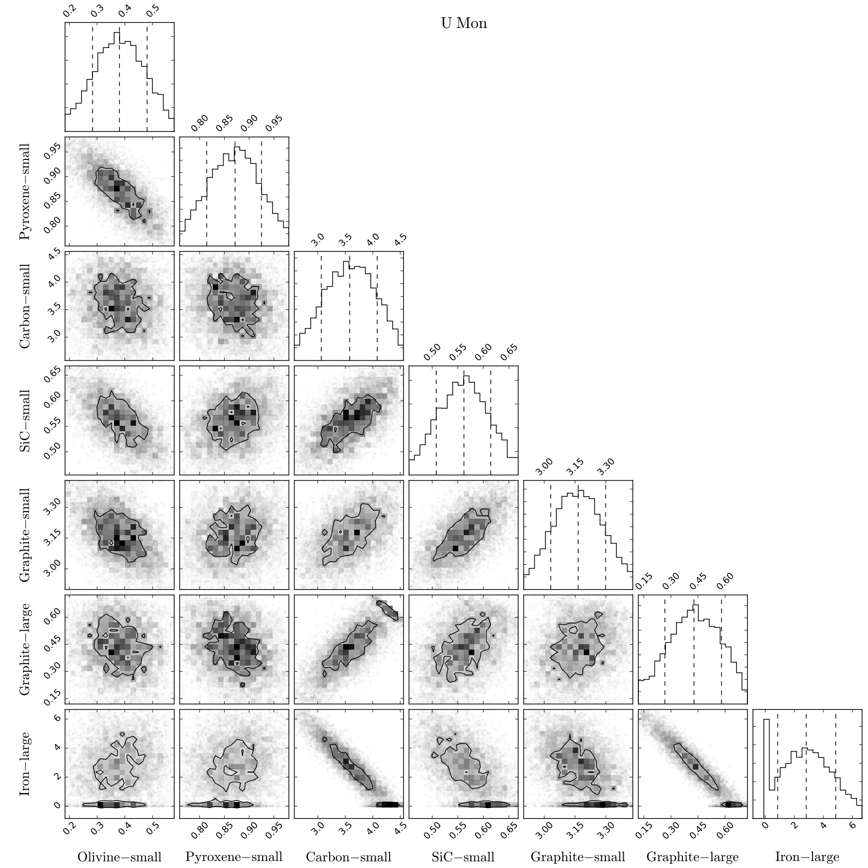
U Mon
Pyroxene−small
Carbon−small
SiC−small
Graphite−small
Graphite−large
Iron−large
Olivine−small
Pyroxene−small
Carbon−small
SiC−small
Graphite−small
Graphite−large
Iron−large

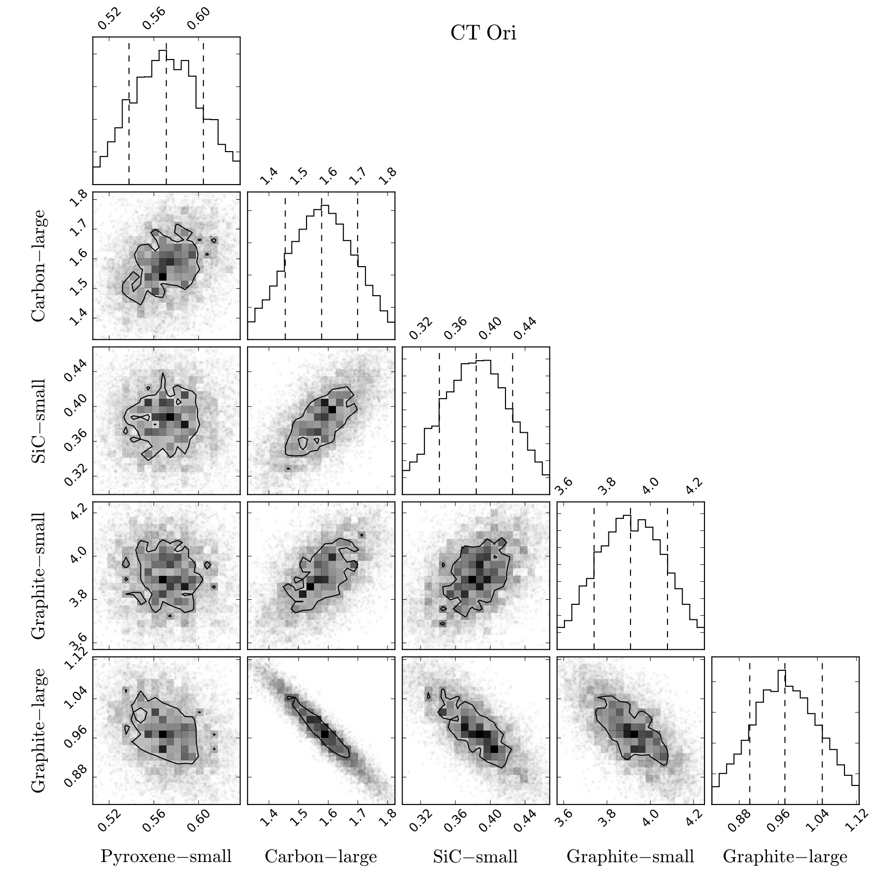
CT Ori
Carbon−large
SiC−small
Graphite−small
Graphite−large
Pyroxene−small
Carbon−large
SiC−small
Graphite−small
Graphite−large

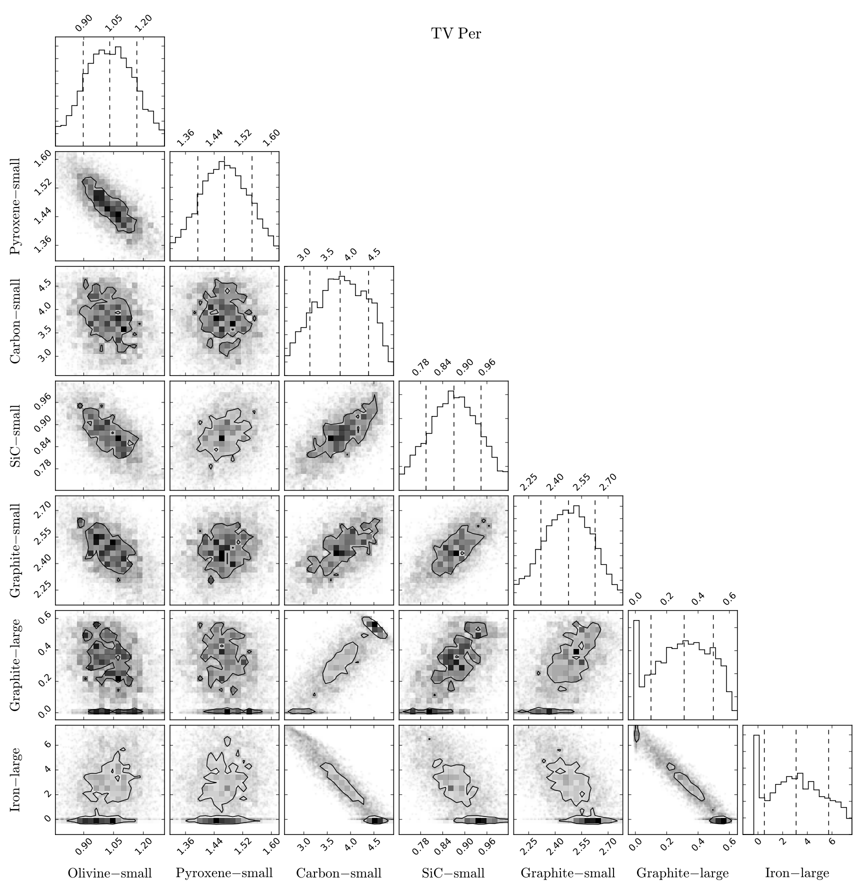
TV Per
Pyroxene−small
Carbon−small
SiC−small
Graphite−small
Graphite−large
Iron−large
Olivine−small
Pyroxene−small
Carbon−small
SiC−small
Graphite−small
Graphite−large
Iron−large

TX Per

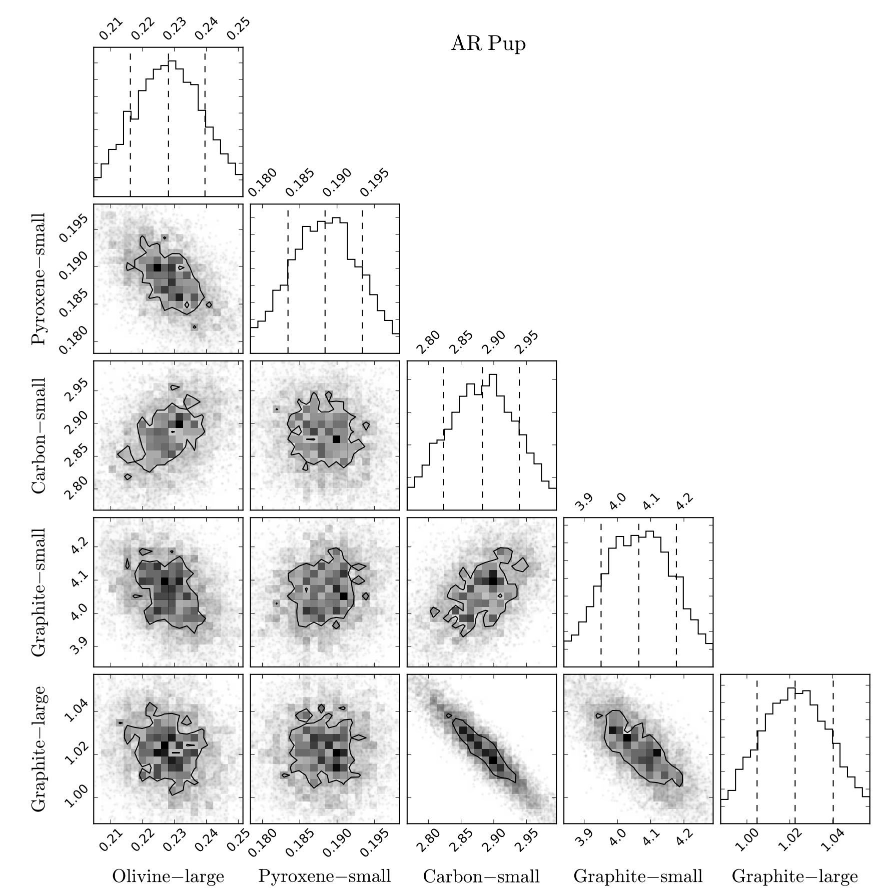
AR Pup
Pyroxene−small
Carbon−small
Graphite−small
Graphite−large
Olivine−large
Pyroxene−small
Carbon−small
Graphite−small
Graphite−large

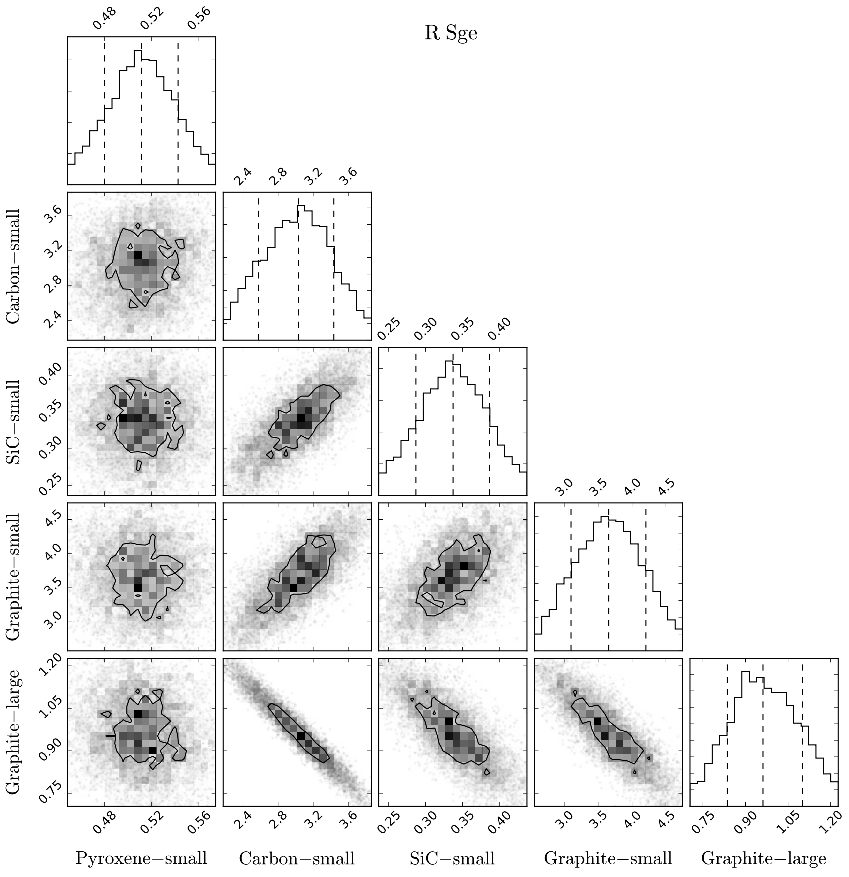
R Sge
Pyroxene−small
Carbon−small
SiC−small
Graphite−small
Graphite−large

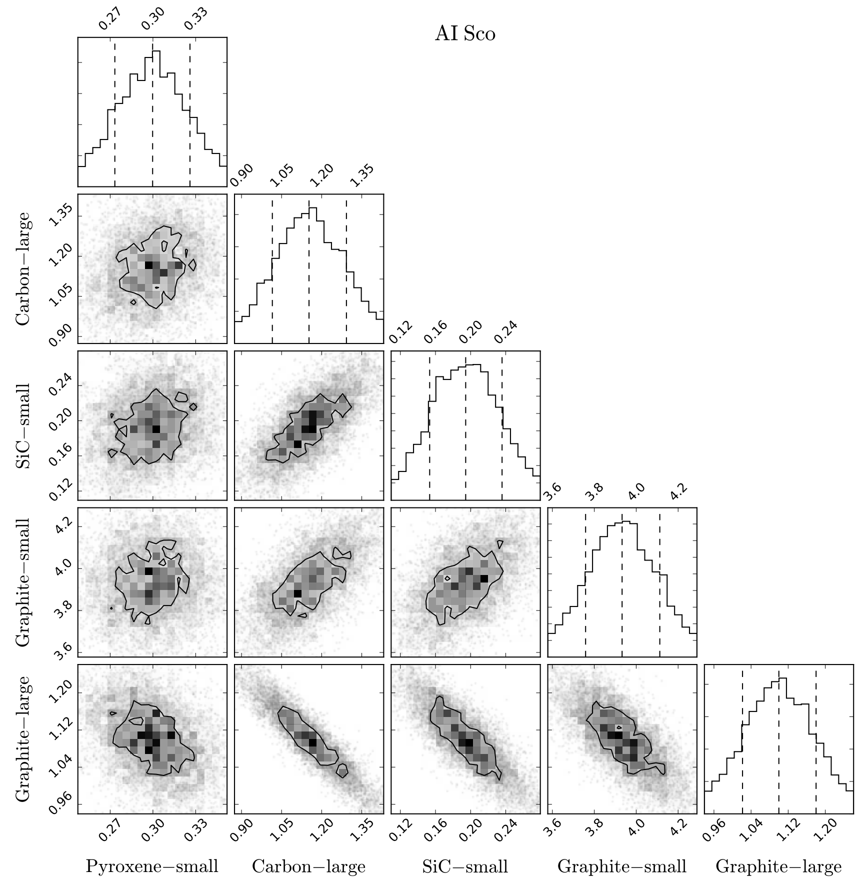
AI Sco
Pyroxene−small
Carbon−large
SiC−small
Graphite−small
Graphite−large

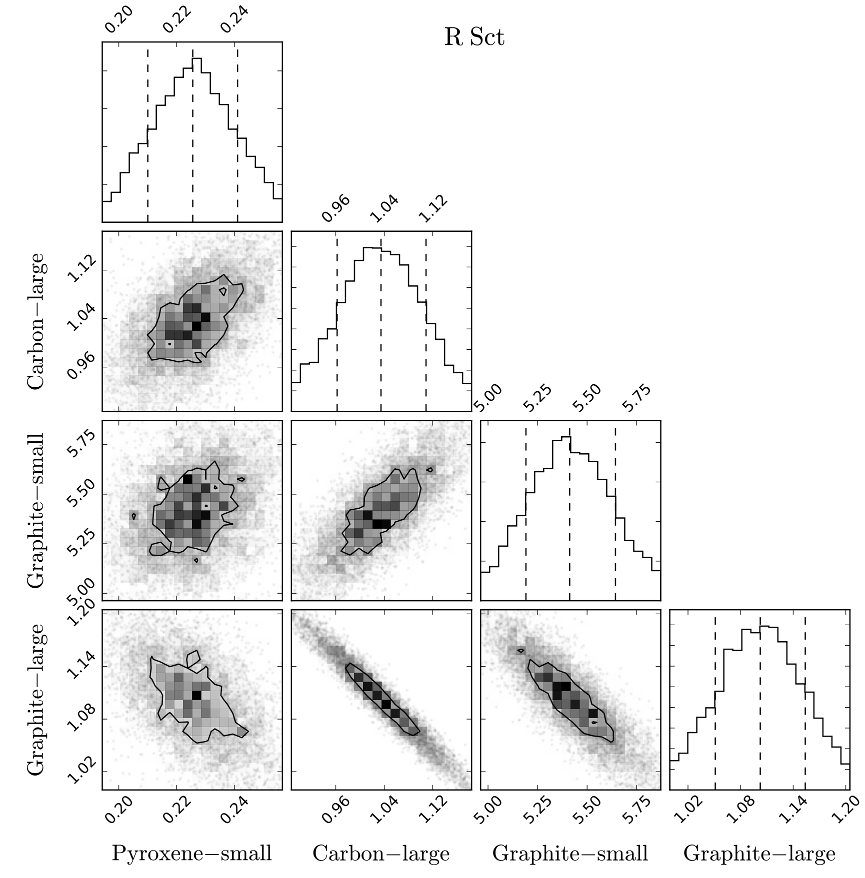
R Sct
Pyroxene−small
Carbon−large
Graphite−small
Graphite−large

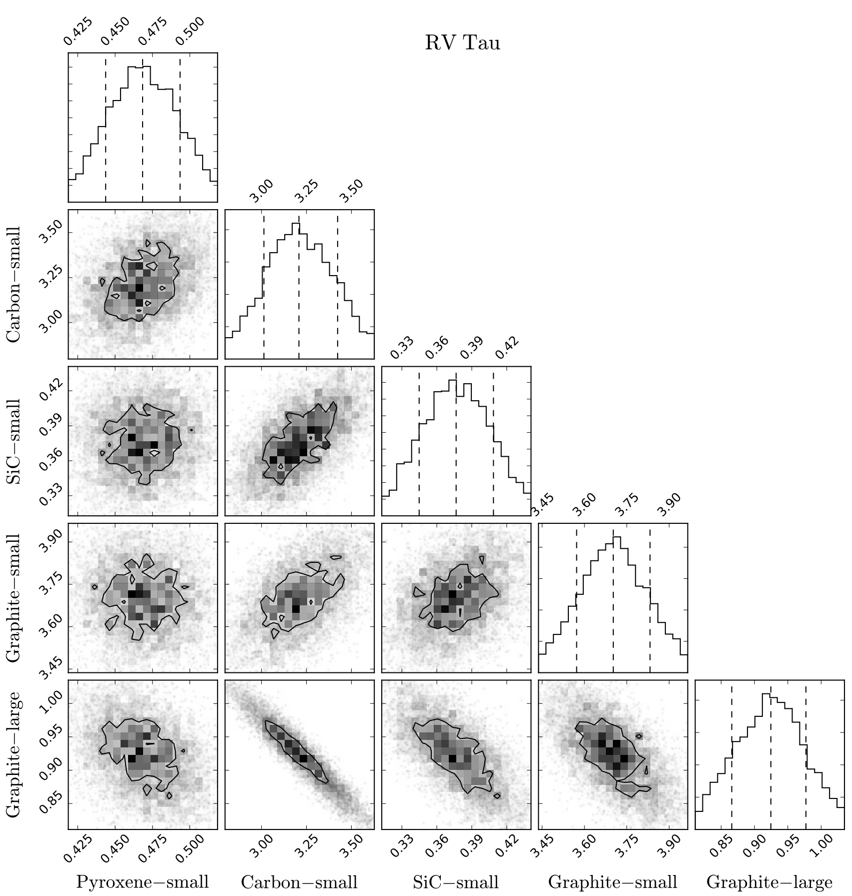
RV Tau
Pyroxene−small
Carbon−small
SiC−small
Graphite−small
Graphite−large

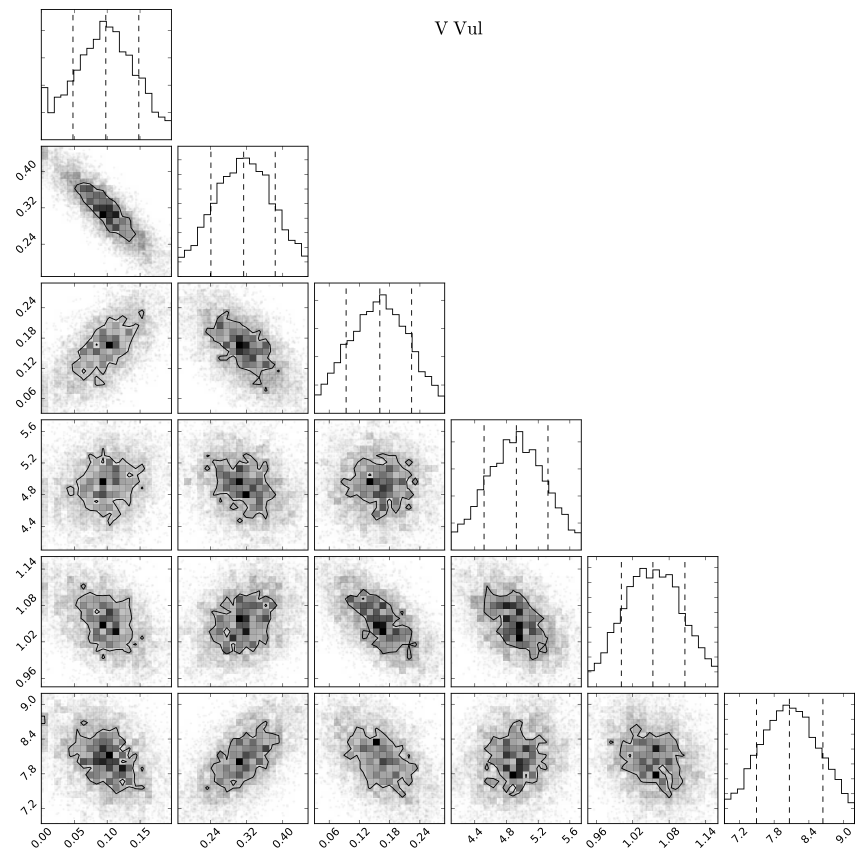
V Vul

Removing Species: High Signal-to-noise

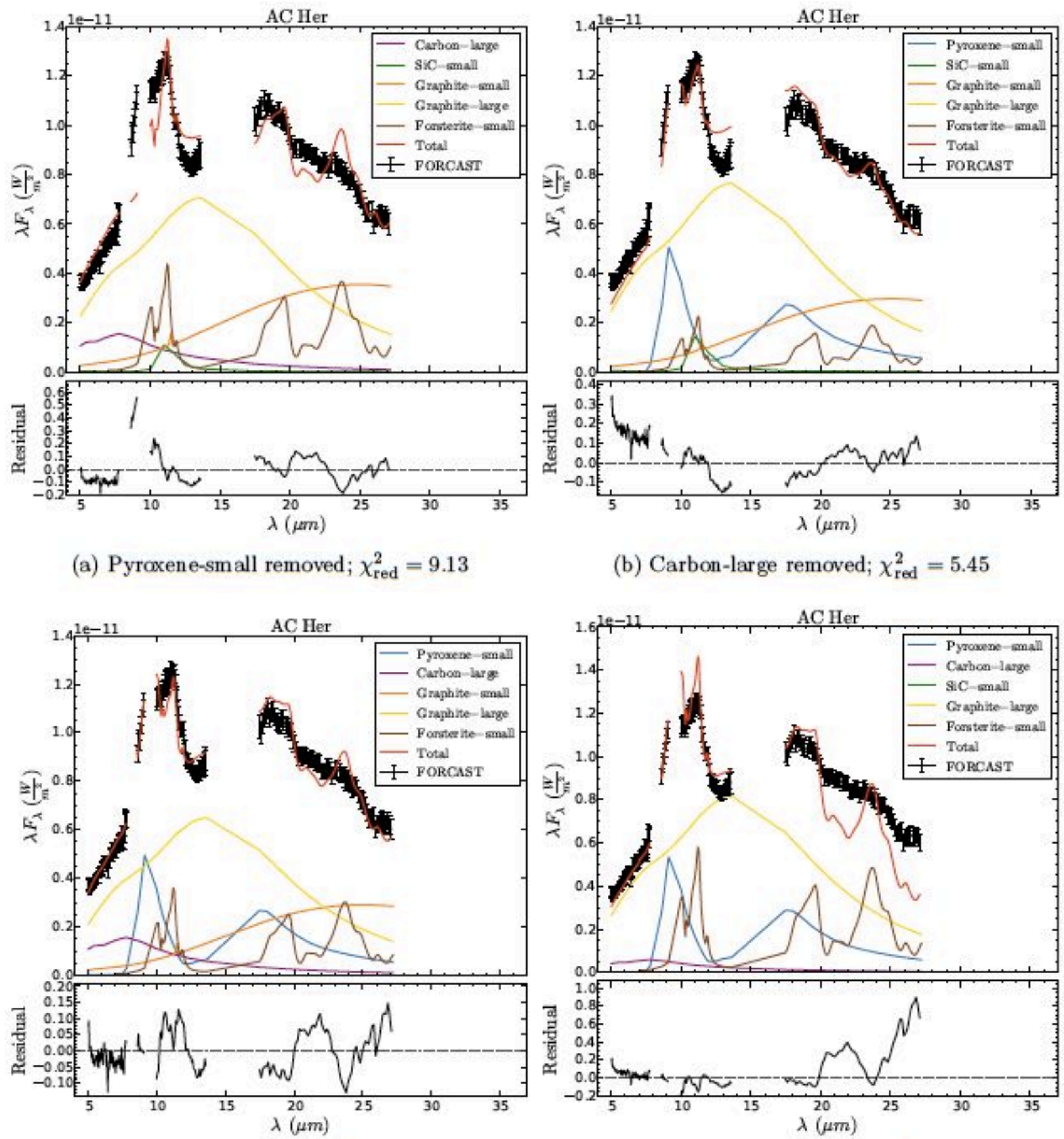

(a) Pyroxene-small removed; $\chi^2_{red} = 9.13$

(b) Carbon-large removed; $\chi^2_{red} = 5.45$

(c) SiC-small removed; $\chi^2_{red} = 2.37$

(d) Graphite-small removed; $\chi^2_{red} = 10.2$

Adding Species: High Signal-to-noise

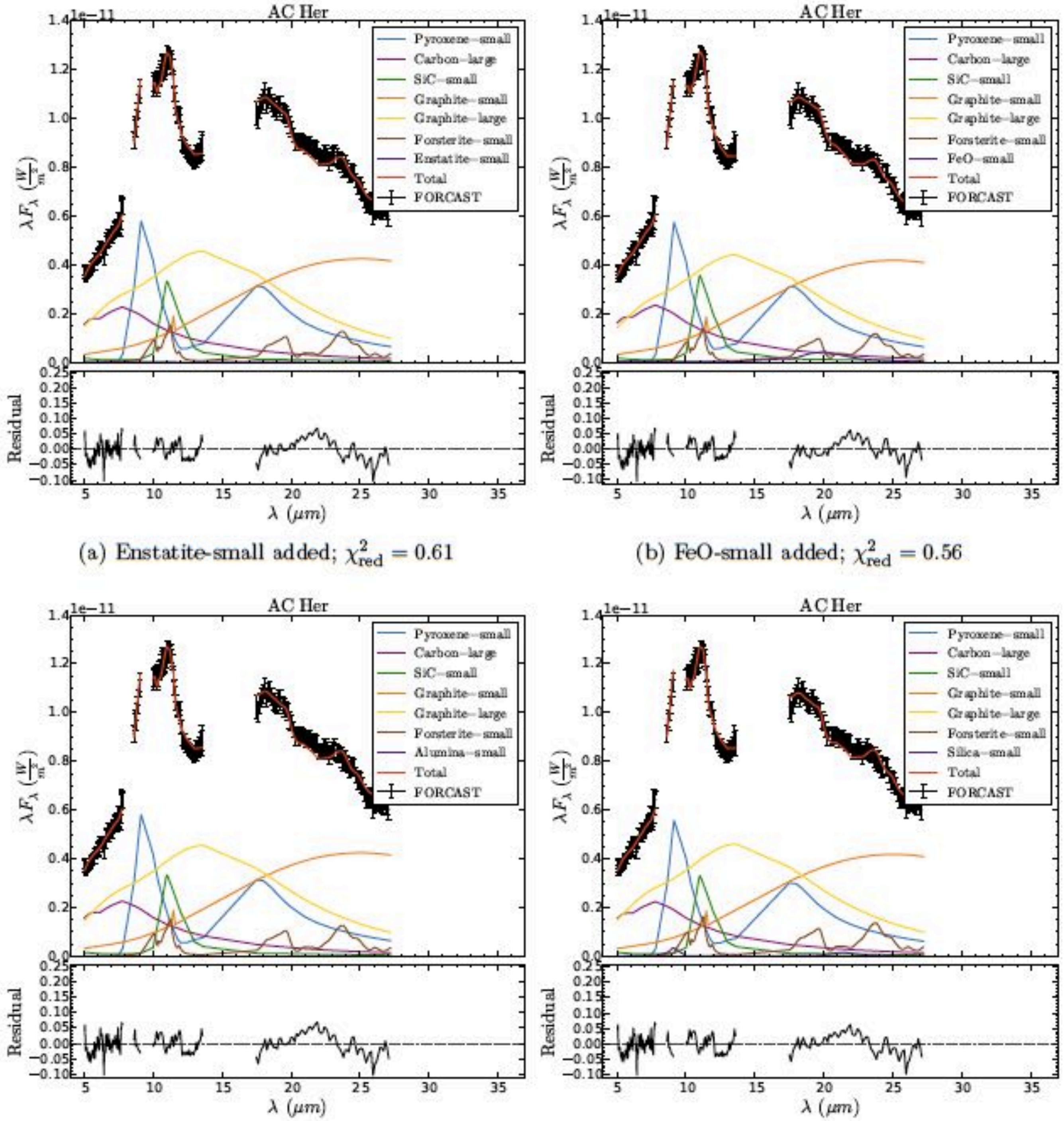

(a) Enstatite-small added; $\chi^2_{\mathrm{red}} = 0.61$

(b) FeO-small added; $\chi^2_{\mathrm{red}} = 0.56$

(c) Alumina-small added; $\chi^2_{\mathrm{red}} = 0.61$

(d) Silica-small added; $\chi^2_{\mathrm{red}} = 0.59$

Removing Species: Low Signal-to-noise

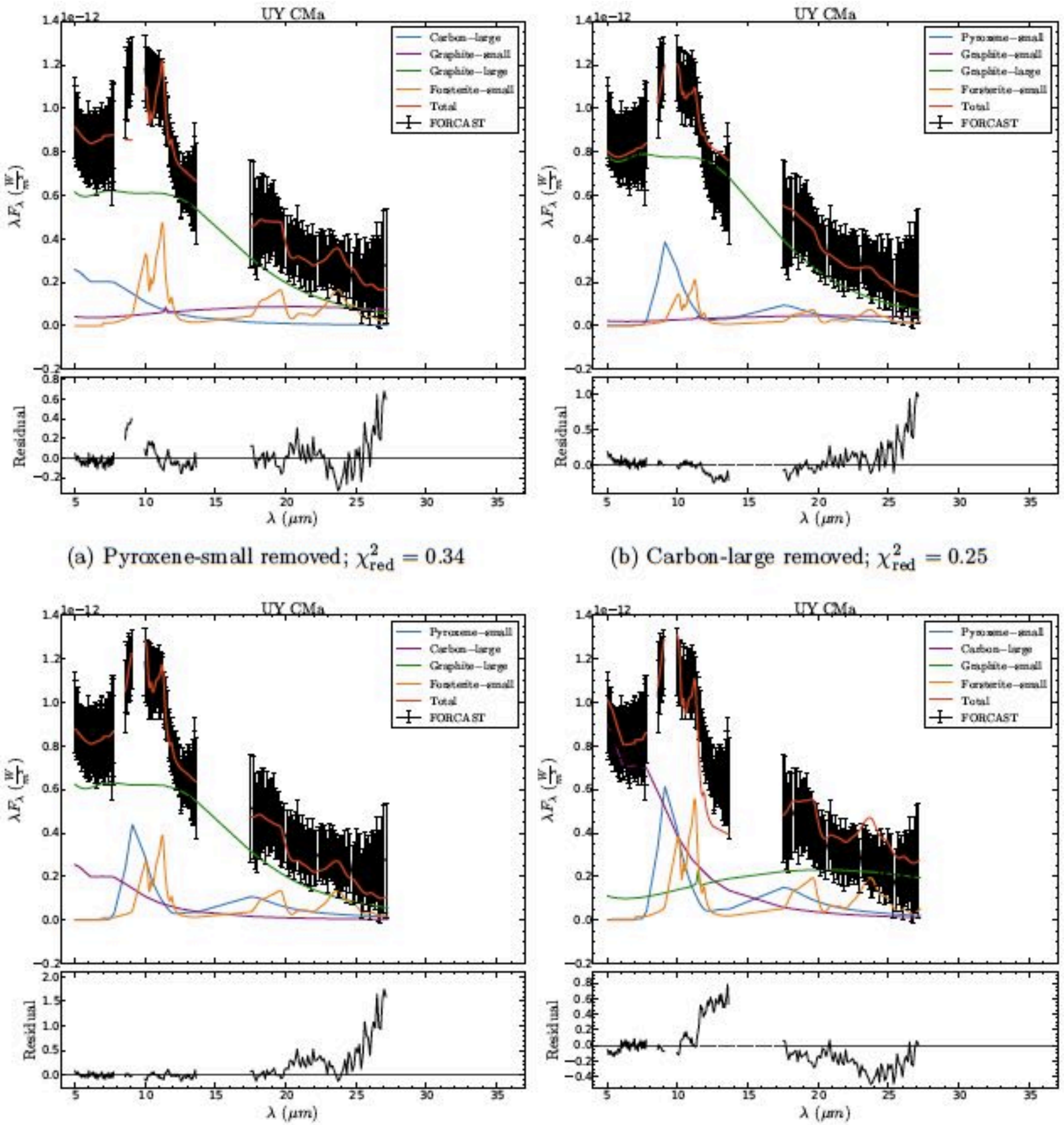

(a) Pyroxene-small removed; $\chi^2_{\text{red}} = 0.34$

(b) Carbon-large removed; $\chi^2_{\text{red}} = 0.25$

(c) Graphite-small removed; $\chi^2_{\text{red}} = 0.14$

(d) Graphite-large removed; $\chi^2_{\text{red}} = 0.90$

Adding Species: Low Signal-to-noise

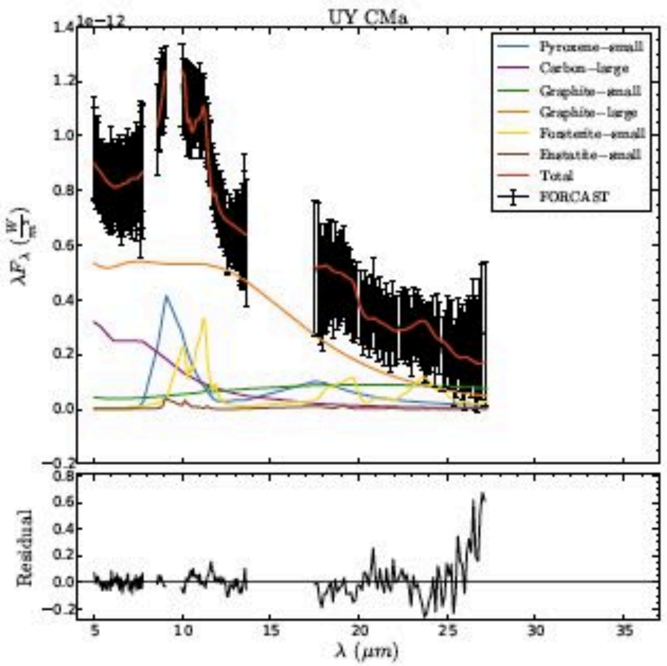

(a) Enstatite-small added; $\chi^2_{\mathrm{red}} = 0.085$

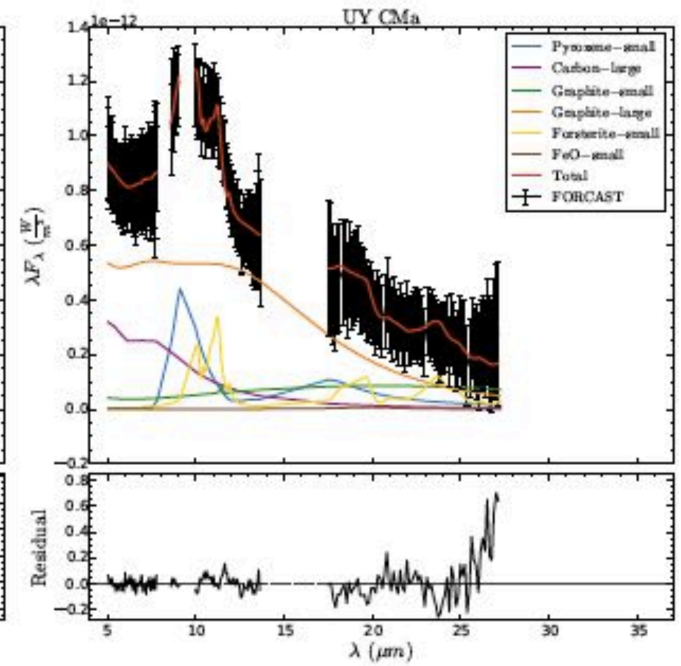

(b) FeO-small added; $\chi^2_{\mathrm{red}} = 0.085$

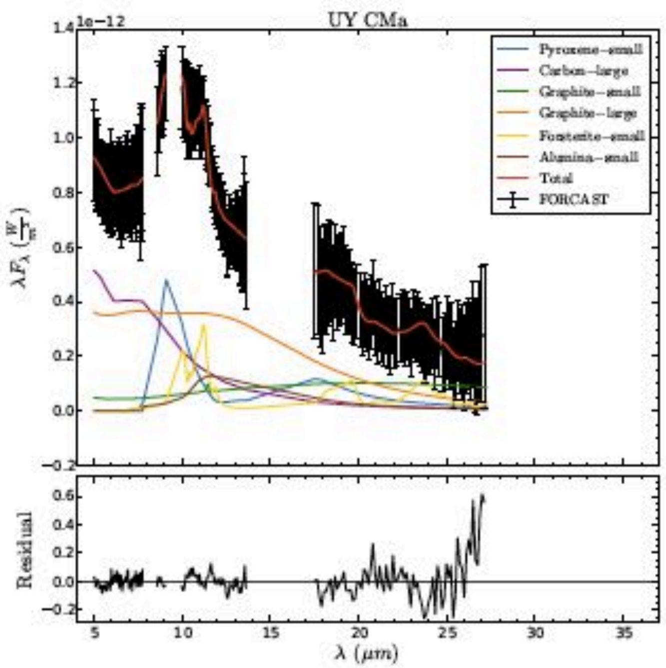

(c) Alumina-small added; $\chi^2_{\mathrm{red}} = 0.080$

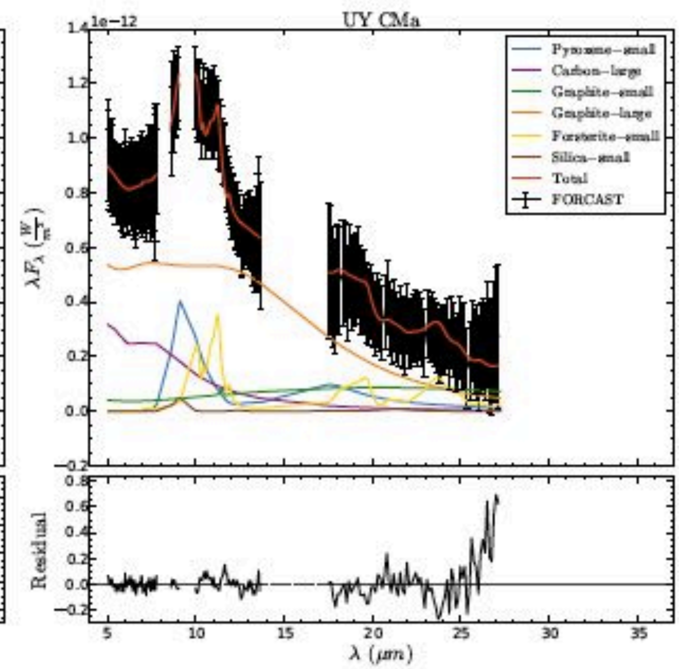

(d) Silica-small added; $\chi^2_{\mathrm{red}} = 0.085$

Conclusions

- Most of the continua are well described by two Planck functions; at ~1000 K and ~250 K with a majority of the dust (97%) in the cooler form
- Our models predict both C-rich and O-rich minerals
- Majority of the dust is in the form of amorphous carbon and graphite (80±1%)
- FORCAST spectra don't exhibit strong crystalline features;
  UY CMa, RU Can and AC Her have forsterite volume fractions of 4±0.9%, 1±0.3% and 1±0.1%, respectively
- On average, the SRd variables contain 8% more small-carbon dust than the RV Tauri stars; the volume fraction of large grains for the SRd variables was 16% and 30% for RV Tauri stars
- Between the featureless IR dust species, amorphous carbon is included in more of our models (16 out of 17) than metallic iron (4 out of 17).